65 $(CH_3)_3NCH_2COO \cdot H_3PO_4$ family

65A Pure compounds

No. 65A-1 $(CH_3)_3NCH_2COO \cdot H_3PO_4$, Betaine phosphate (BP)

(M = 215.14; [D: 229.23])

1a Antiferroelectricity in $(CH_3)_3NCH_2COO \cdot H_3PO_4$ was discovered by Albers et al. in 1982. 82Alb

b

phase	IV	III	II	I
state	A	A	P	P
crystal system	monoclinic	monoclinic	monoclinic	monoclinic
space group	$P2_1/c - C_{2h}^5$	$P2_1/c - C_{2h}^5$ *)	$P2_1/c - C_{2h}^5$ [a])	$P2_1/m - C_{2h}^2$
Θ [K]	81 [b]) [D: 155		86 [b])	365 [b]) 365···367 K] **)

[a]) 84Sch, 89Hay

[b]) 82Alb

*) Another space group, $P2_1$, has also been reported for phase III. 95San

**) $(CH_3)_3NCH_2COO \cdot D_3PO_4$. [c]) [d]) For crystals deuterated more than about 90 %, the phase III has been reported to disappear. [e]) [f]) For 89 % deuterated crystal, Θ_{III-II} = 142.6 K and Θ_{IV-III} = 139 K. [f])

[c]) 84Alb
[d]) 84Sch
[e])90Kro
[f]) 88Bru

Antiferroelectric axis || [010]. 82Alb

$\rho = 1.463 \cdot 10^3$ kg m^{-3}, $\rho_X = 1.469 \cdot 10^3$ kg m^{-3}. 82Alb

Colorless. 82Alb

Cleavage plane: (001), $(10\bar{2})$. 82Alb

T_{melt} = 480 K. 82Alb

2a Crystal growth: slow evaporation of aqueous solution. 84Alb

b Direction of crystallographic axes (a, b, c) and cleavage planes: Fig. 65A-1-001.

3a Unit cell parameters: Table 65A-1-001; see also Fig. 65B-2-003 in No. 65B-2.
$a = a_0$, $b = b_0$, $c = 2c_0$, $\beta = \beta_0$ in phase II and III, $a = 2a_0$, $b = b_0$, $c = 2c_0$, $\beta = \beta_0$ in phase III, where a_0, b_0, c_0, β_0 are lattice parameters in phase I. 89Hay, 95San

b Z = 2 in phase I, 4 in phase II and phase III, 8 in phase IV. 84Sch, 89Hay

Crystal structure: Fig. 65A-1-002.
Positional and temperature parameters in phases I and II: Table 65A-1-002, Table 65A-1-003.
Interatomic distances and bond angles: Table 65A-1-004.

4 Thermal expansion coefficients: Table 65A-1-005.

5a Dielectric constant: Fig. 65A-1-003, Fig. 65A-1-004, Fig. 65A-1-005.
Curie-Weiss behavior, $\kappa_b = C/(T - \Theta_p)$, 130 K < T < RT, where $C = 1.38 \cdot 10^4$ K and Θ_p = 72 K. 82Alb
Dielectric dispersion: Fig. 65A-1-006, Fig. 65A-1-007, Fig. 65A-1-008.
Dielectric dispersion of deuterated crystal: Fig. 65A-1-009, Fig. 65A-1-010, Fig. 65A-1-011.
Effect of p on κ_b: Fig. 65A-1-012.
$d\Theta_{III-II}/dp = -0.065$ K MPa^{-1}. 94Lan

	$\Theta - p$ phase diagram: Fig. 65A-1-013.	
	$\Theta - E_{bias}$ phase diagram: Fig. 65A-1-014, Fig. 65A-1-015; see also	91Kro
b	Effect of E_{bias} on κ_b: Fig. 65A-1-016, Fig. 65A-1-017, Fig. 65A-1-018. Effect of E_{bias} on dielectric dispersion: Fig. 65A-1-019, Fig. 65A-1-020, Fig. 65A-1-021.	
c	Sublattice polarization and critical field: Fig. 65A-1-022, Fig. 65A-1-023, Fig. 65A-1-024. Sublattice polarization and critical field of deuterated crystal: Fig. 65A-1-025, Fig. 65A-1-026, Fig. 65A-1-027.	
6a	Specific heat: Fig. 65A-1-028, Fig. 65A-1-029. Transition entropy: $\Delta S_{III-II} + \Delta S_{IV-III} = 0.40$ J K^{-1} mol^{-1}.	89Mae
8a	Elastic stiffness and compliance: Table 65A-1-006; Fig. 65A-1-030; see also Table 65A-2-003 in No. 65A-2. Sound velocity: Fig. 65A-1-031, Fig. 65A-1-032.	
9a	Principal refractive indices: $n_\alpha = 1.470(1)$ (|| [010]), $n_\beta = 1.493(1)$, $n_\gamma = 1.540(1)$ for $\lambda = 589$ nm at 293 K. For principal axes of optical indicatrix, see Fig. 65A-1-001 in 2b. Optical axial angle: $2V = 73°$ for $\lambda = 589$ nm at 293 K. Indicatrix rotation: Fig. 65A-1-033. Birefringence: Fig. 65A-1-034. Effect of E_{bias} on birefringence: Fig. 65A-1-035. Infrared reflection spectra: see Mode frequencies determined from infrared reflectivity data: Table 65A-1-007. κ'' spectra calculated from infrared reflectivity data: Fig. 65A-1-036.	82Alb 82Alb 97San
10a	Raman scattering: see	85Fre, 88Bru, 89Har
11	Electrical conductivity of deuterated crystal: Fig. 65A-1-037.	
13a	NMR of ^{1}H and ^{31}P: Fig. 65A-1-038. NMR of ^{2}H: see	 95Fre, 96Fre, 98Fre
b	ESR of γ-irradiated crystal: see	92Vol
14a	Bragg reflections: Fig. 65A-1-039, Fig. 65A-1-040, Fig. 65A-1-041. See also Fig. 65B-1-013 in No. 65B-1.	
b	X-ray critical scattering around Θ_{II-I}: Fig. 65A-1-042.	

Table 65A-1-001. $(CH_3)_3NCH_2COO \cdot H_3PO_4$ (BP), $(CH_3)_3NCH_2COO \cdot (H_{0.1}D_{0.9})_3PO_4$. Unit cell parameters [84Sch].

	$(CH_3)_3NCH_2COO \cdot H_3PO_4$		$(CH_3)_3NCH_2COO \cdot (H_{0.1}D_{0.9})_3PO_4$		
T [K]	383 (phase I)	295 (phase II)	294 (phase II)	150 (phase II)	113 (phase III)
a [Å]	11.114(4)	11.076(4)	11.079	11.066	22.126
b [Å]	7.907(3)	7.852(3)	7.852	7.810	7.798
c [Å]	6.543(3)	12.944(6)	12.922	12.766	12.704
β [°]	119.77(2)	119.62(2)	119.51	119.41	119.23
V [Å^3]	499.1	978.6	978.3	961.1	1912.8

Table 65A-1-002. $(CH_3)_3NCH_2COO \cdot H_3PO_4$ (BP). Structure of phase I [84Sch]. Fractional coordinates and temperature parameters. Anisotropic temperature parameters U_{ij} [Å^2] are defined by Eq. (d) in Introduction. (!) means imposed parameters which were not refined. Atoms with fixed fractional coordinates are described by a disordered model; their multiplicities are 0.5, if not otherwise mentioned. Mult.: multiplicity of atom. T = 383 K.

Atom	x	y	z	U_{11}	U_{22}	U_{33}	U_{12}	U_{13}	U_{23}
P	0.3611(1)	0.2539(!)	0.8291(2)	0.051(1)	0.046(1)	0.068(1)	0	0.034(1)	0
O(3)	0.2479(4)	0.2021(2)	0.5821(6)	0.071(2)	0.073(4)	0.077(2)	–0.008(2)	0.041(2)	–0.023(2)
O(4)	0.4875(5)	0.1433(6)	0.9088(9)	0.068(3)	0.074(3)	0.115(4)	0.025(2)	0.062(3)	0.030(3)
O(5)	0.3069(3)	0.2252(!)	0.0041(5)	0.057(2)	0.083(2)	0.072(2)	0	0.038(1)	0
O(6)	0.3973(5)	0.4339(5)	0.8231(8)	0.062(3)	0.054(2)	0.098(3)	–0.006(2)	0.017(2)	0.013(2)
O(1)	0.0411(2)	0.2388(!)	0.8242(5)	0.050(2)	0.133(3)	0.055(2)	0	0.024(1)	0
O(2)	0.9979(3)	0.2517(!)	0.4532(5)	0.061(2)	0.171(3)	0.064(2)	0	0.038(2)	0
C(5)	0.9619(4)	0.2519(!)	0.6079(8)	0.052(2)	0.071(3)	0.062(3)	0	0.028(2)	0
C(4)	0.8079(4)	0.2741(!)	0.5048(8)	0.051(2)	0.040(4)	0.047(3)	0	0.022(2)	0
N	0.7488(3)	0.2678(!)	0.6663(5)	0.052(2)	0.034(2)	0.050(2)	0	0.025(2)	0
C(1)	0.5948(7)	0.2924(!)	0.520(2)	0.055(4)	0.088(9)	0.069(5)	0	0.036(4)	0
C(2)	0.781(4)	0.106(4)	0.805(8)	0.12(2)	0.10(1)	0.12(2)	0.02(1)	0.08(2)	0.00(1)
C(3)	0.792(3)	0.411(3)	0.818(5)	0.07(2)	0.060(8)	0.09(1)	–0.004(7)	0.04(1)	–0.044(9)
H(1)	0.573(4)	0.387(7)	0.416(9)	0.04(1)					
H(2)	0.570(7)	0.25(1)	0.42(1)	0.12(4)					
H(3)	0.555(4)	0.293(!)	0.617(7)	0.07(1)					
H(4)	0.727(5)	0.098(!)	0.89(1)	0.05(1)					
H(5)	0.72(1)	0.008(!)	0.66(2)	0.15(3)					
H(6)	0.860(7)	0.086(!)	0.88(1)	0.02(2)					
H(7)	0.80(1)	0.404(!)	0.95(2)	0.13(5)					
H(8)	0.907(6)	0.387(!)	0.96(1)	0.07(2)					
H(9)	0.800(8)	0.519(!)	0.76(1)	0.10(2)					
H(10)	0.784(5)	0.370(6)	0.432(9)	0.04(1)					
H(11)	0.754(4)	0.196(6)	0.376(8)	0.05(2)					
H(12)	0.179(!)	0.223(!)	0.549(!)	0.087(!)	Mult. = 0.283(!)				
H(12")	0.077(!)	0.235(!)	0.504(!)	0.103(!)	Mult. = 0.217(!)				
H(13)	0.489(!)	0.065(!)	0.962(!)	0.040(!)	Mult. = 0.25(!)				
H(14)	0.230(!)	0.231(!)	0.953(!)	0.139(!)					
H(15)	0.451(!)	0.462(!)	0.909(!)	0.078(!)	Mult. = 0.25(!)				

Table 65A-1-003. $(CH_3)_3NCH_2COO \cdot (H_{0.1}D_{0.9})_3PO_4$. Structure of phase II [84Sch]. Fractional coordinates and temperature parameters. Anisotropic temperature parameters U_{ij} [Å^2] are defined by Eq. (d) in Introduction. The multiplicities of the disordered hydrogens are indicated. Mult.: multiplicity of atom. (!) means imposed parameters which were not refined. T = 294 K.

Atom	x	y	z	U_{11}	U_{22}	U_{33}	U_{12}	U_{13}	U_{23}
P	0.3595(1)	0.2531(1)	0.4137(1)	0.0313(4)	0.0288(4)	0.0421(8)	–0.0010(5)	0.0189(4)	0.0006(5)
O(3)	0.2459(2)	0.2014(3)	0.2894(3)	0.042(2)	0.055(2)	0.045(2)	–0.003(1)	0.019(1)	–0.015(1)
O(4)	0.4890(3)	0.1446(4)	0.4543(3)	0.042(2)	0.042(2)	0.073(2)	0.014(1)	0.037(1)	0.014(2)
O(5)	0.3071(2)	0.2258(3)	0.5042(2)	0.039(1)	0.063(2)	0.046(2)	0.007(1)	0.027(1)	0.008(1)
O(6)	0.3952(3)	0.4390(3)	0.4116(3)	0.042(2)	0.030(1)	0.065(2)	–0.003(1)	0.010(2)	0.010(1)
O(1)	0.0396(2)	0.2412(4)	0.4121(2)	0.033(1)	0.099(2)	0.027(2)	0.003(2)	0.014(1)	0.001(2)
O(2)	0.9973(2)	0.2512(4)	0.2241(3)	0.036(1)	0.118(2)	0.039(3)	0.006(2)	0.022(1)	–0.001(2)
C(5)	0.9625(3)	0.2513(5)	0.3041(4)	0.038(2)	0.046(2)	0.036(4)	–0.003(2)	0.021(2)	–0.004(3)
C(4)	0.8057(3)	0.2713(5)	0.2505(4)	0.037(2)	0.040(2)	0.034(3)	–0.001(2)	0.016(2)	0.002(2)
N	0.7475(2)	0.2645(4)	0.3328(2)	0.032(1)	0.037(2)	0.028(2)	0.002(1)	0.016(1)	0.003(2)
C(1)	0.5924(4)	0.2863(7)	0.2569(5)	0.035(2)	0.081(4)	0.049(4)	0.006(2)	0.023(2)	0.011(3)
C(2)	0.7736(5)	0.0957(5)	0.3949(5)	0.054(3)	0.044(3)	0.056(4)	0.001(2)	0.026(3)	0.014(2)
C(3)	0.8025(5)	0.4048(6)	0.4238(5)	0.072(3)	0.044(3)	0.043(4)	0.000(2)	0.035(3)	–0.009(2)
H(1)	0.576(3)	0.397(5)	0.214(3)	0.09(1)					
H(2)	0.559(3)	0.198(5)	0.201(3)	0.10(2)					
H(3)	0.553(3)	0.286(4)	0.313(3)	0.07(1)					
H(4)	0.717(3)	0.087(5)	0.440(3)	0.10(2)					
H(5)	0.743(3)	0.005(5)	0.329(3)	0.10(1)					
H(6)	0.867(3)	0.092(4)	0.446(3)	0.06(1)					
H(7)	0.745(3)	0.403(4)	0.464(3)	0.08(1)					
H(8)	0.908(3)	0.375(5)	0.479(3)	0.10(1)					
H(9)	0.785(3)	0.508(5)	0.381(3)	0.08(1)					
H(10)	0.784(3)	0.377(4)	0.208(3)	0.05(1)					
H(11)	0.773(3)	0.184(4)	0.199(3)	0.06(1)					
H(12)	0.184(6)	0.246(9)	0.266(6)	0.05(2)	Mult. = 0.56(4)				
H(12")	0.073(7)	0.227(7)	0.250(6)	U(H12)	Mult. = 0.44				
H(13)	0.494(8)	0.062(7)	0.459(6)	0.05(3)	Mult. = 0.5(!)				
H(14)	0.231(3)	0.233(5)	0.479(3)	0.06(1)					
H(15)	0.471(6)	0.452(9)	0.452(6)	0.05(3)	Mult. = 0.5(!)				

Table 65A-1-004. $(CH_3)_3NCH_2COO \cdot (H_{0.1}D_{0.9})_3PO_4$. Structure at T = 150 K (phase II) [84Sch]. Interatomic distances [Å] and bond angles [°]. $\Theta_{III–II}$ = 146 K.

Distance [Å]		Angle [°]	
P–O(3)	1.533(2)	O(3)–P–O(4)	111.5(1)
P–O(4)	1.532(2)	O(4)–P–O(5)	107.2(1)
P–O(5)	1.567(3)	O(5)–P–O(6)	109.9(1)
P–O(6)	1.533(2)	O(6)–P–O(4)	109.6(1)
C(5)–O(1)	1.246(3)	O(1)–C(5)–O(2)	126.9(2)
C(5)–O(2)	1.272(4)	O(2)–C(5)–C(4)	111.6(2)
C(5)–O(4)	1.529(3)	O(1)–C(5)–C(4)	121.6(3)
C(4)–N	1.507(4)	C(5)–C(4)–N	117.7(2)
C(3)–N	1.512(3)	C(3)–N–C(4)	112.1(2)
C(2)–N	1.516(3)	C(2)–N–C(4)	111.6(2)
C(1)–N	1.514(3)	C(1)–N–C(4)	106.8(2)
C(1)–H(1)	1.02(2)	C(1)–N–C(2)	108.2(2)
C(1)–H(2)	1.01(2)	C(1)–N–C(3)	108.2(2)
C(1)–H(3)	0.96(4)	N–C(1)–H(3)	108.7(12)
C(2)–H(4)	1.03(3)	C(2)–N–C(3)	109.8(2)
C(2)–H(5)	0.97(2)	N–C(2)–H(5)	109.0(14)
C(2)–H(6)	0.96(2)	N–C(2)–H(6)	109.0(13)
C(3)–H(7)	1.03(3)	N–C(3)–H(7)	106.6(12)
C(3)–H(8)	0.96(2)	N–C(3)–H(8)	108.3(14)
C(3)–H(9)	0.97(2)	N–C(3)–H(9)	110.1(14)
C(4)–H(10)	0.97(2)	N–C(4)–H(10)	107.5(16)
C(4)–H(11)	0.98(2)	N–C(4)–H(11)	108.3(17)
O(3)–H(12)	0.78(5)	P–O(3)–H(12)	114.0(31)
O(2)–H(12")	0.73(7)	C(5)–O(2)–H(12")	117.4(51)
O(4)–H(13)	0.73(4)	P–O(4)–H(13)	114.8(39)
O(5)–H(14)	0.72(3)	P–O(5)–H(14)	110.0(38)
O(6)–H(15)	0.63(4)	P–O(6)–H(15)	112.1(43)
O(2)–O(3)	2.470(3)	O(2)–H(12)–O(3)	168.8(45)
O(1)–O(5)	2.609(2)	O(1)–H(14)–O(5)	174.6(36)
O(4)–O(4)	2.533(3)	O(4)–H(13)–O(4)	171.6(60)
O(6)–O(6)	2.514(3)	O(6)–H(15)–O(6)	169.1(62)
H(12)–H(12")	0.97(8)	P–O(3)–O(2)	121.7(1)
H(13)–H(13)	1.11(7)	P–O(4)–O(4)	120.6(1)
H(15)–H(15)	1.28(8)	P–O(6)–O(6)	117.3(1)

Table 65A-1-005. $(CH_3)_3NCH_2COO \cdot H_3PO_4$ (BP), $(CH_3)_3NCH_2COO \cdot H_3PO_3$ (BPI). Thermal expansion coefficients [$\cdot 10^{-6}$ K^{-1}] at RT [89Hau]. Estimated limits of error: $3 \cdot 10^{-6}$ K^{-1}. $\boldsymbol{X}_1 \perp \boldsymbol{b}$ and $\boldsymbol{c}$, $\boldsymbol{X}_2 \parallel \boldsymbol{b}$, $\boldsymbol{X}_3 \parallel \boldsymbol{c}$.

	α_{11}	α_{22}	α_{33}	α_{13}
BP	9	56	73	15
BPI	50	16	53	–36

Table 65A-1-006. $(CH_3)_3NCH_2COO \cdot H_3PO_4$ (BP), $(CH_3)_3NCH_2COO \cdot H_3PO_3$ (BPI). Elastic properties at RT [89Hau]. $c_{\lambda\mu}$: elastic stiffness constants [$\cdot 10^{10}$ N m^{-2}], K^{-1}: inverse bulk compressibility [$\cdot 10^{10}$ N m^{-2}]. $\boldsymbol{X}_1 \perp \boldsymbol{b}$ and $\boldsymbol{c}$, $\boldsymbol{X}_2 \parallel \boldsymbol{b}$, $\boldsymbol{X}_3 \parallel \boldsymbol{c}$. Estimated limits of error: c_{11}, c_{22}, c_{33}: 0.3 %; c_{44}, c_{55}, c_{66}, K^{-1}: 1 %; c_{12}, c_{13}, c_{23}: 3 %; other $c_{\lambda\mu}$: $<0.06 \cdot 10^{10}$ N m^{-2}.

	BP	BPI
c_{11}	2.945	1.284
c_{22}	1.966	1.862
c_{33}	1.366	1.714
c_{44}	0.622	0.443
c_{55}	0.357	0.363
c_{66}	0.304	0.485
c_{12}	1.118	0.757
c_{13}	1.132	0.922
c_{23}	0.815	1.084
c_{15}	–0.419	–0.099
c_{25}	–0.025	–0.054
c_{35}	–0.384	–0.198
c_{46}	0.136	0.200
K^{-1}	1.090	1.025

Table 65A-1-007. $(CH_3)_3NCH_2COO \cdot H_3PO_4$ (BP). Frequencies of the vibrational modes [cm^{-1}] and their assignments [97San]. Based on infrared reflectivity data.

Frequency [cm^{-1}]	Assignment
Internal modes of the betaine molecule	
2990	C–H stretching
2350	C–O stretching
1750	C=O
1460	N–C stretching (ν_3)
920	N–C bending (ν_4)
Internal modes of the phosphate tetrahedra	
800–900	Stretching (ν_3)
400–450	Bending (ν_4)

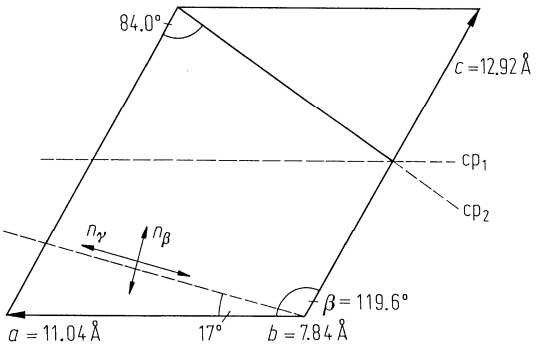

Fig. 65A-1-001. $(CH_3)_3NCH_2COO \cdot H_3PO_4$ (BP). Directions of crystallographic axes (*a*, *b*, *c*) and principal axes of optical indicatrix (n_β, n_γ) [82Alb]. cp_1 and cp_2 indicate two cleavage planes parallel to (001) and $(10\bar{2})$.

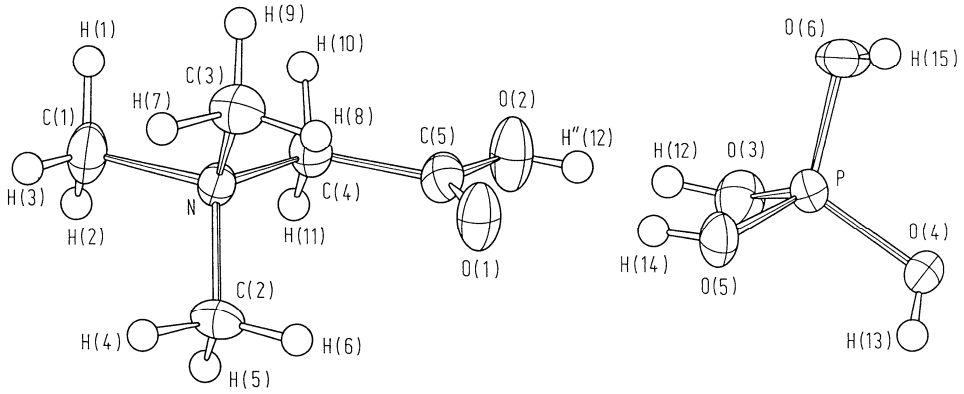

Fig. 65A-1-002. $(CH_3)_3NCH_2COO \cdot (H_{0.1}D_{0.9})_3PO_4$. Crystal structure [84Sch]. Asymmetric unit in phase II. $T = 150$ K. $\Theta_{III-II} = 146$ K.

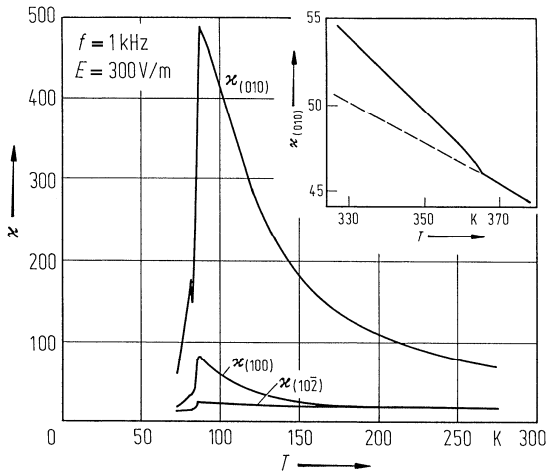

Fig. 65A-1-003. $(CH_3)_3NCH_2COO \cdot H_3PO_4$ (BP). $\kappa_{(100)}$, $\kappa_{(010)}$, $\kappa_{(10\bar{2})}$ vs. *T* [82Alb]. *f* = 1 kHz.

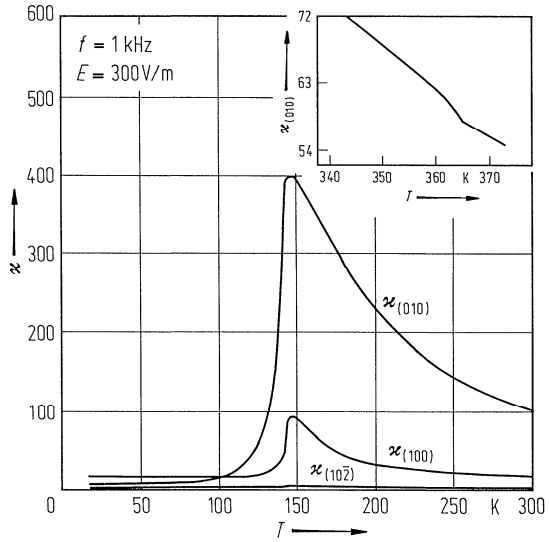

Fig. 65A-1-004. $(CH_3)_3NCH_2COO \cdot (H_{0.1}D_{0.9})_3PO_4$. $\kappa_{(100)}$, $\kappa_{(010)}$, $\kappa_{(10\bar{2})}$ vs. T [84Alb]. f = 1 kHz.

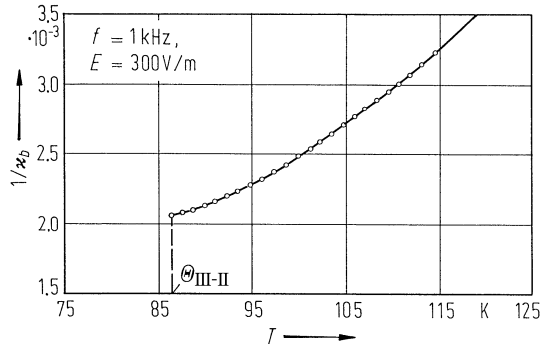

Fig. 65A-1-005. $(CH_3)_3NCH_2COO \cdot H_3PO_4$ (BP). $1/\kappa_b$ vs. T [82Alb]. f = 1 kHz.

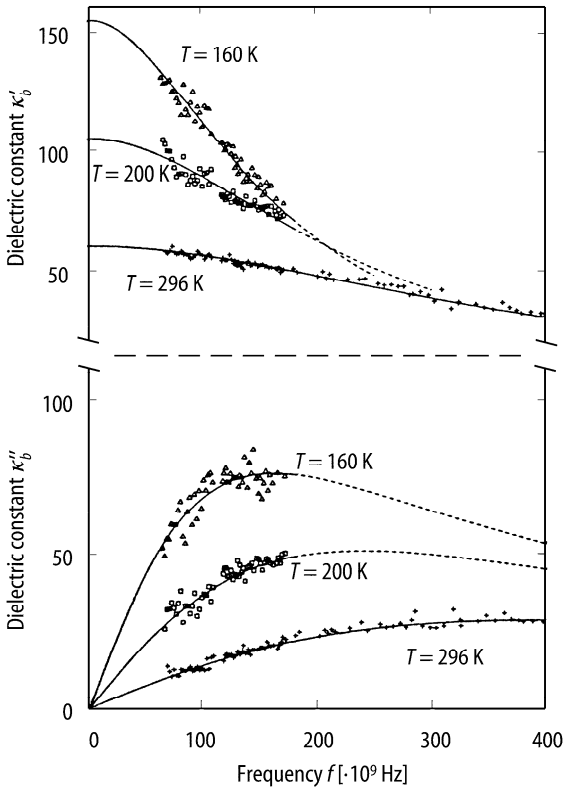

Fig. 65A-1-006. $(CH_3)_3NCH_2COO \cdot H_3PO_4$ (BP). κ'_b, κ''_b vs. f in phase II [90Fis]. Parameter: T. The curves are fits of the Debye dispersion formula.

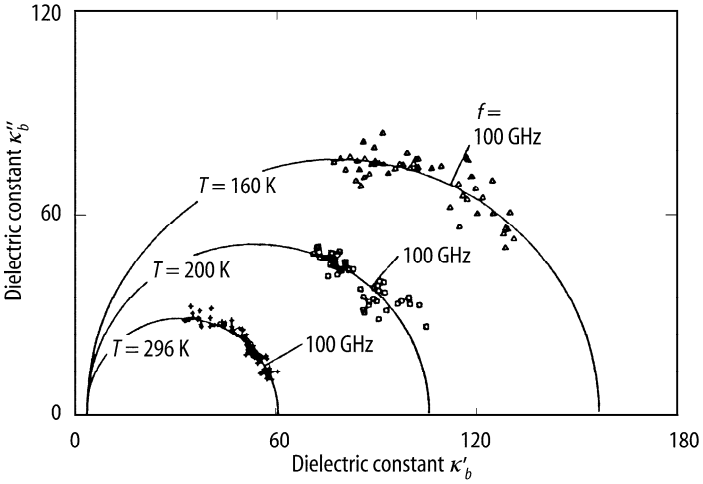

Fig. 65A-1-007. $(CH_3)_3NCH_2COO \cdot H_3PO_4$ (BP). Cole-Cole diagram of complex dielectric constants in phase II [90Fis]. Parameter: T. The circular arcs are fits of the Debye dispersion formula.

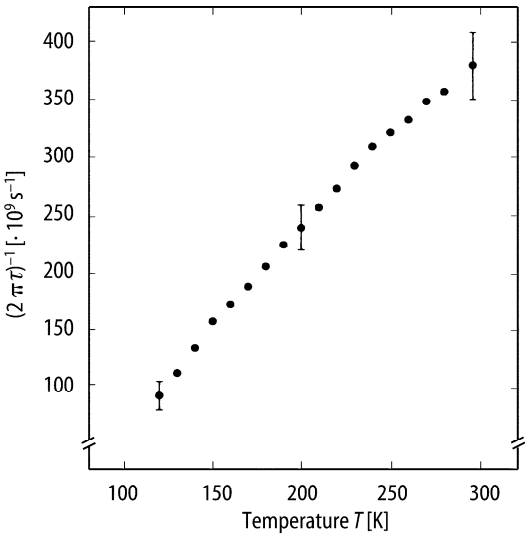

Fig. 65A-1-008. $(CH_3)_3NCH_2COO \cdot H_3PO_4$ (BP). $(2\pi\tau)^{-1}$ vs. T [90Fis]. τ: dielectric relaxation time.

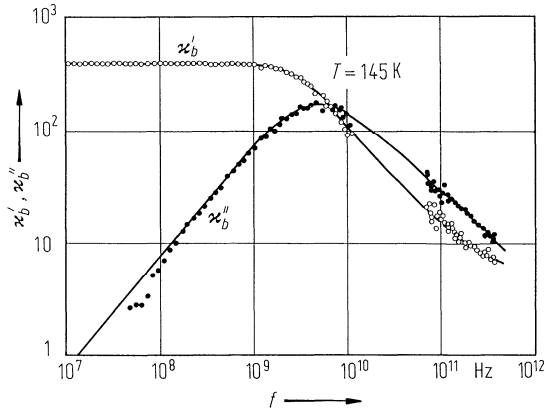

Fig. 65A-1-009. $(CH_3)_3NCH_2COO \cdot (H_{0.11}D_{0.89})_3PO_4$. κ_b', κ_b'' vs. f [88Bru]. T = 145 K. Solid lines are fits of the Cole-Davidson formula.

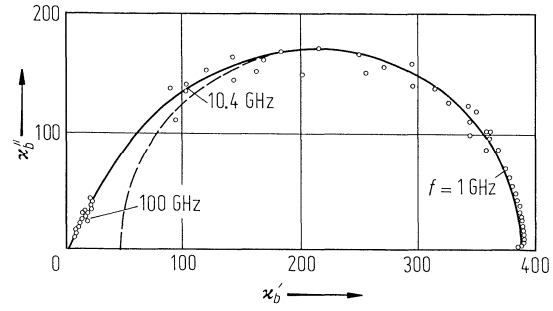

Fig. 65A-1-010. $(CH_3)_3NCH_2COO \cdot (H_{0.11}D_{0.89})_3PO_4$. Cole-Cole plot of complex dielectric constant [88Bru]. Solid lines are fits of the Cole-Davidson formula, and broken curve is a fit of Debye dispersion formula. T = 145 K.

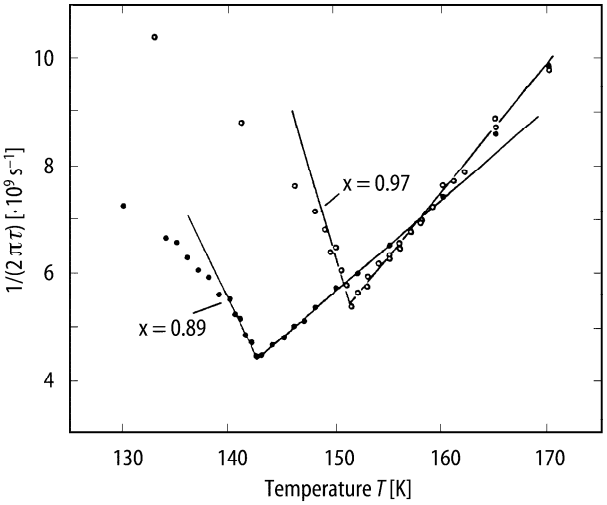

Fig. 65A-1-011. $(CH_3)_3NCH_2COO \cdot (H_{0.11}D_{0.89})_3PO_4$ (DBP). $(2\pi\tau)^{-1}$ vs. T [88Bru]. Parameter: x. τ: dielectric relaxation time.

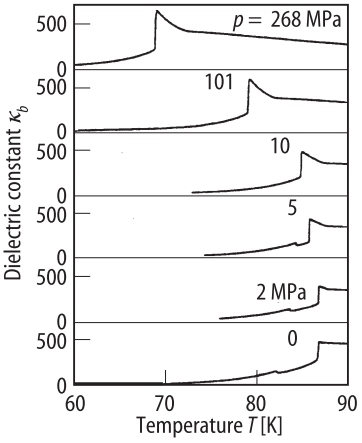

Fig. 65A-1-012. $(CH_3)_3NCH_2COO \cdot H_3PO_4$ (BP). κ_b vs. T [92Lau]. Parameter: p.

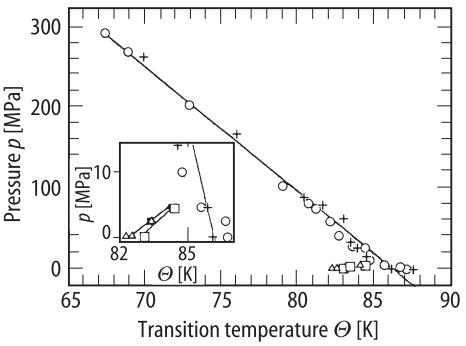

Fig. 65A-1-013. $(CH_3)_3NCH_2COO \cdot H_3PO_4$ (BP). Θ vs. p [92Lau]. Plus, open square: on heating; open circle, open triangle: on cooling.

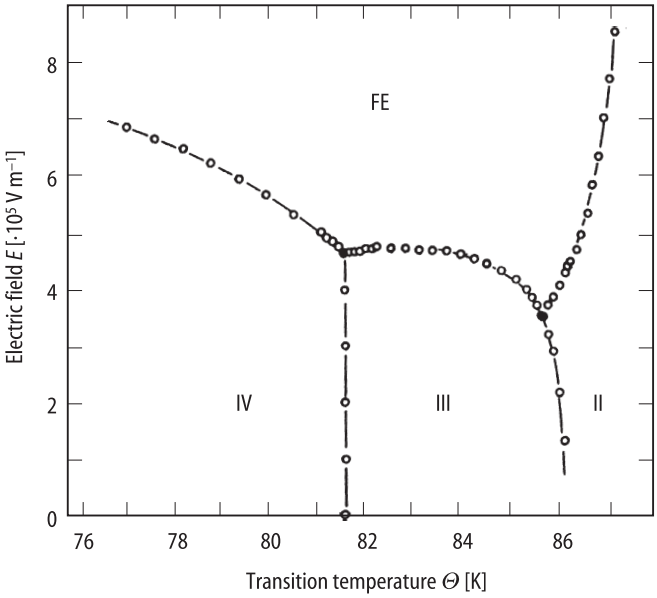

Fig. 65A-1-014. $(CH_3)_3NCH_2COO \cdot H_3PO_4$ (BP). $\Theta - E$ phase diagram [89Suz]. Obtained from dielectric constant measurements. FE: ferroelectric phase induced by electric field.

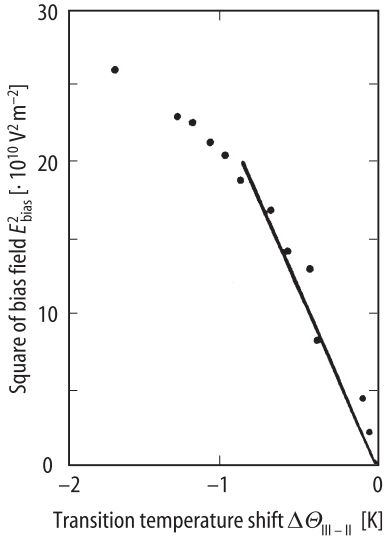

Fig. 65A-1-015. $(CH_3)_3NCH_2COO \cdot H_3PO_4$ (BP). E^2_{bias} vs. $\Delta\Theta_{III-II}$ [89Har]. $\Delta\Theta_{III-II}$: shift of Θ_{III-II}.

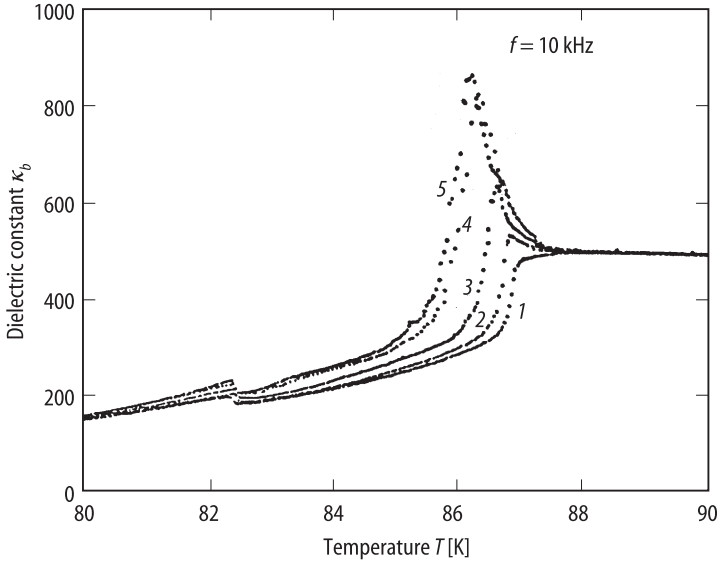

Fig. 65A-1-016. $(CH_3)_3NCH_2COO \cdot H_3PO_4$ (BP). κ_b vs. T [89Har]. Parameter: E_{bias}. *1*: $E_{bias} = 0$, *2*: $2.85 \cdot 10^5$ V m^{-1}, *3*: $3.77 \cdot 10^5$ V m^{-1}, *4*: $4.34 \cdot 10^5$ V m^{-1}, *5*: $4.52 \cdot 10^5$ V m^{-1}.

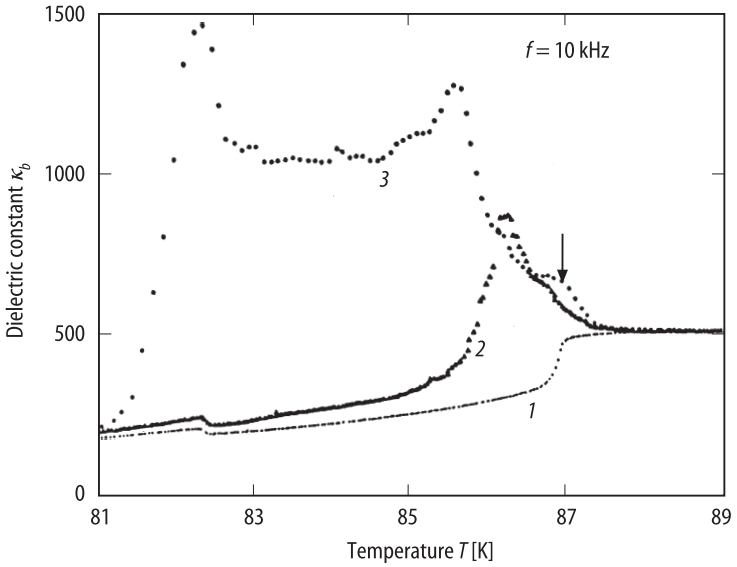

Fig. 65A-1-017. $(CH_3)_3NCH_2COO \cdot H_3PO_4$ (BP). κ_b vs. T [89Har]. Parameter: E_{bias}. *1*: $E_{bias} = 0$, *2*: $4.5 \cdot 10^5$ V m^{-1}, *3*: $5.2 \cdot 10^5$ V m^{-1}. Arrow indicates the field induced phase transition. See Fig. 65A-1-014.

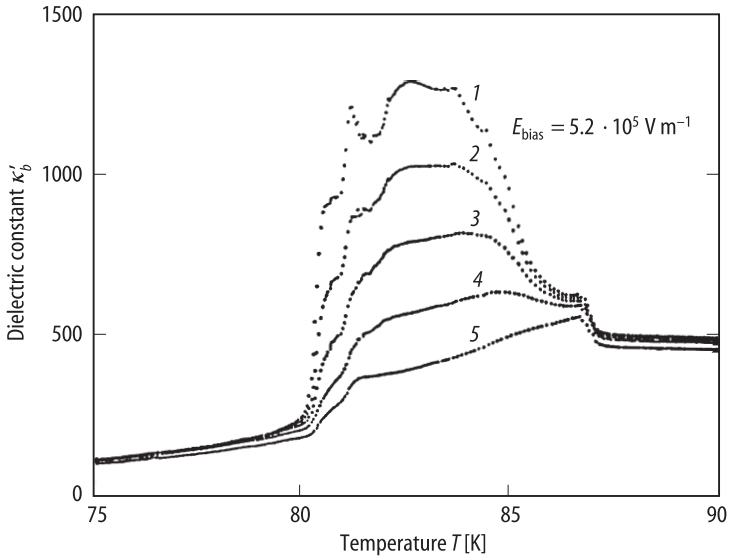

Fig. 65A-1-018. $(CH_3)_3NCH_2COO \cdot H_3PO_4$ (BP). κ_b' vs. T [89Har]. Measurements were made under $E_{bias} = 5.2 \cdot 10^5$ V m^{-1}. Parameter: *f. 1*: f = 10 kHz, *2*: 20 kHz, *3*: 40 kHz, *4*: 100 kHz, *5*: 1 MHz.

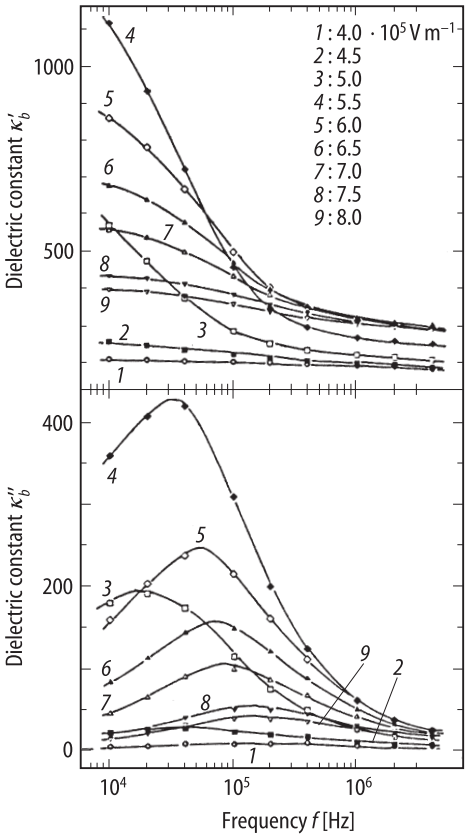

Fig. 65A-1-019. $(CH_3)_3NCH_2COO \cdot H_3PO_4$ (BP). κ_b', κ_b'' vs. f [94Yas]. Parameter: E_{bias}. T = 81.1 K.

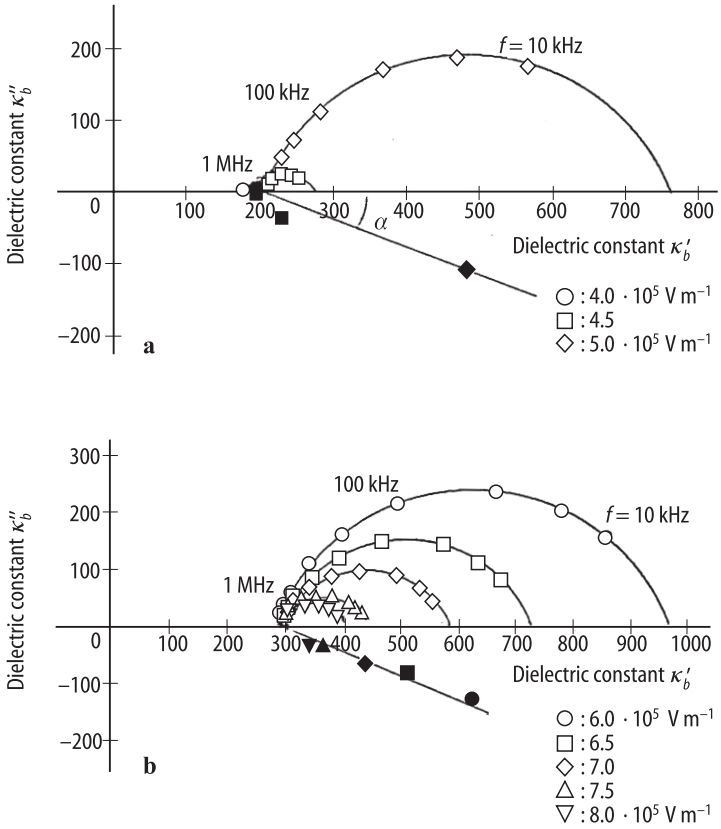

Fig. 65A-1-020. $(CH_3)_3NCH_2COO \cdot H_3PO_4$ (BP). Cole-Cole diagrams of complex dielectric constants [94Yas]. Parameter: E_{bias}. Closed marks indicate the centers of the circular arcs. T = 81.1 K. (**a**) antiferroelectric phase, (**b**) ferroelectric phase induced by electric field.

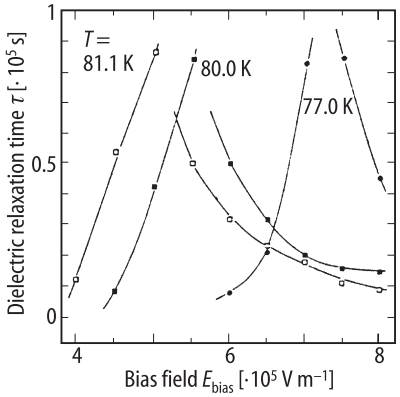

Fig. 65A-1-021. $(CH_3)_3NCH_2COO \cdot H_3PO_4$ (BP). τ vs. E_{bias} [94Yas]. Parameter: T. τ: dielectric relaxation time.

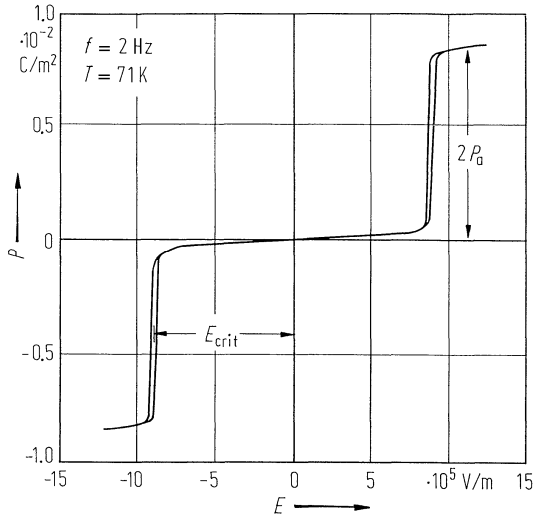

Fig. 65A-1-022. $(CH_3)_3NCH_2COO \cdot H_3PO_4$ (BP). P vs. E [82Alb]. f = 2 Hz, T = 71 K. P_a: sublattice polarization, E_{crit}: critical field.

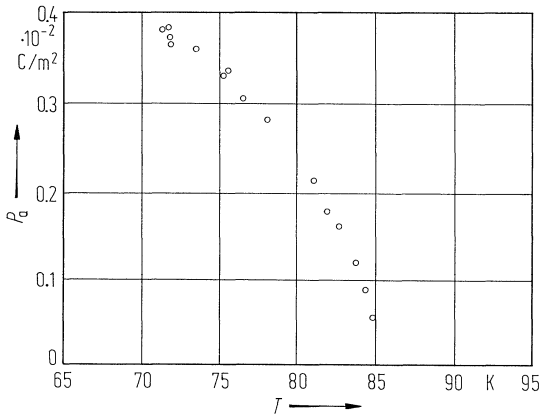

Fig. 65A-1-023. $(CH_3)_3NCH_2COO \cdot H_3PO_4$ (BP). P_a vs. T [82Alb]. P_a: sublattice polarization defined in Fig. 65A-1-022.

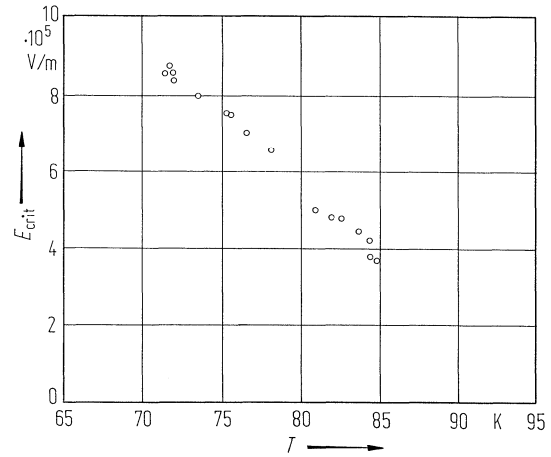

Fig. 65A-1-024. $(CH_3)_3NCH_2COO \cdot H_3PO_4$ (BP). E_{crit} vs. T [82Alb]. E_{crit}: critical field defined in Fig. 65A-1-022.

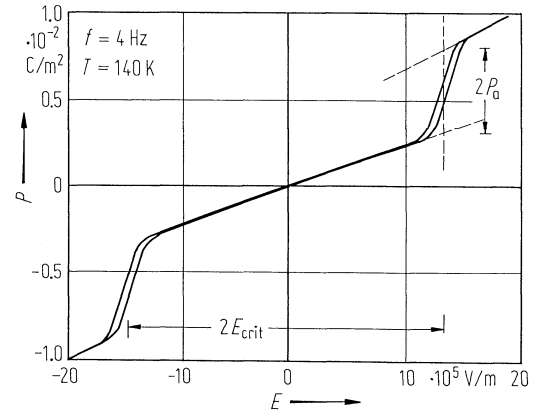

Fig. 65A-1-025. $(CH_3)_3NCH_2COO \cdot (H_{0.1}D_{0.9})_3PO_4$. P vs. E [84Alb]. P_a: sublattice polarization, E_{crit}: critical field. $f = 4$ Hz. $T = 140$ K.

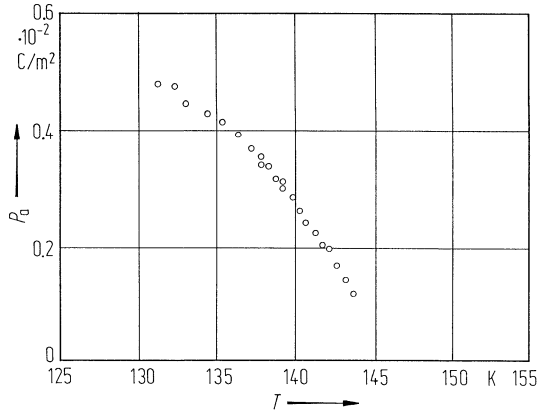

Fig. 65A-1-026. $(CH_3)_3NCH_2COO \cdot (H_{0.1}D_{0.9})_3PO_4$. P_a vs. T [84Alb]. P_a: sublattice polarization defined in Fig. 65A-1-025.

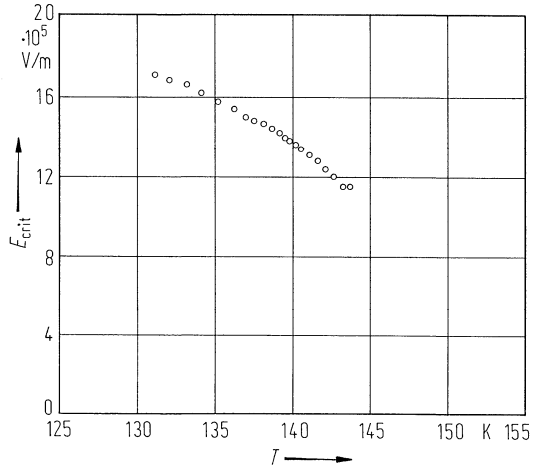

Fig. 65A-1-027. $(CH_3)_3NCH_2COO \cdot (H_{0.1}D_{0.9})_3PO_4$. E_{crit} vs. T [84Alb]. E_{crit}: critical field defined in Fig. 65A-1-025.

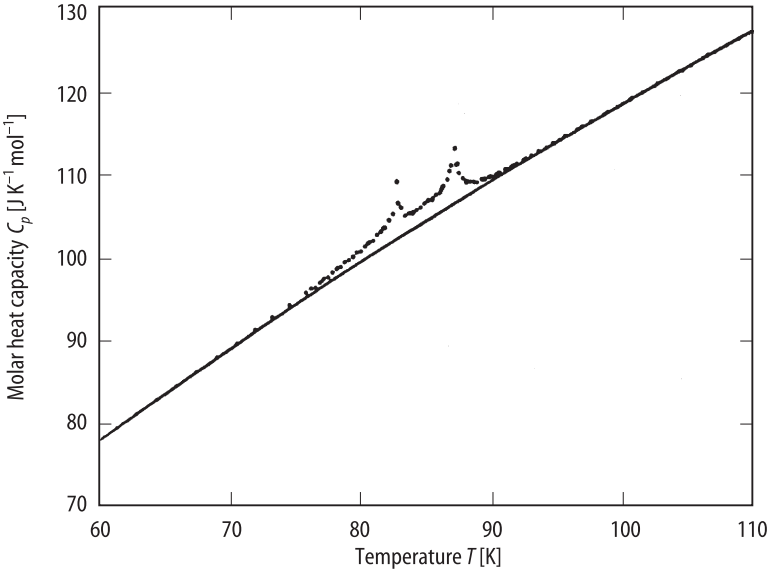

Fig. 65A-1-028. $(CH_3)_3NCH_2COO \cdot H_3PO_4$ (BP). C_p vs. T [89Mae]. C_p: molar heat capacity at constant pressure.

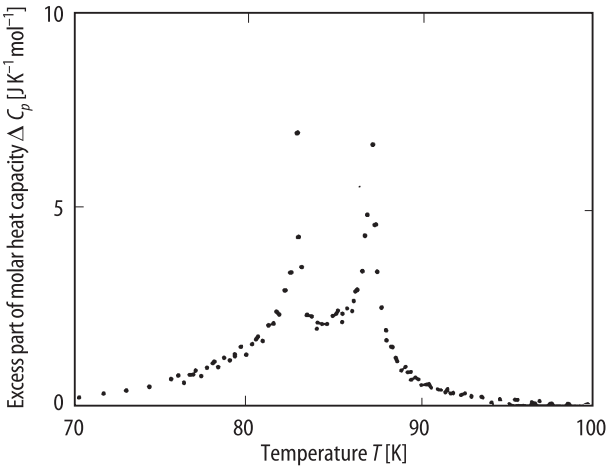

Fig. 65A-1-029. $(CH_3)_3NCH_2COO \cdot H_3PO_4$ (BP). ΔC_p vs. T [89Mae]. ΔC_p: excess part of molar heat capacity at constant pressure.

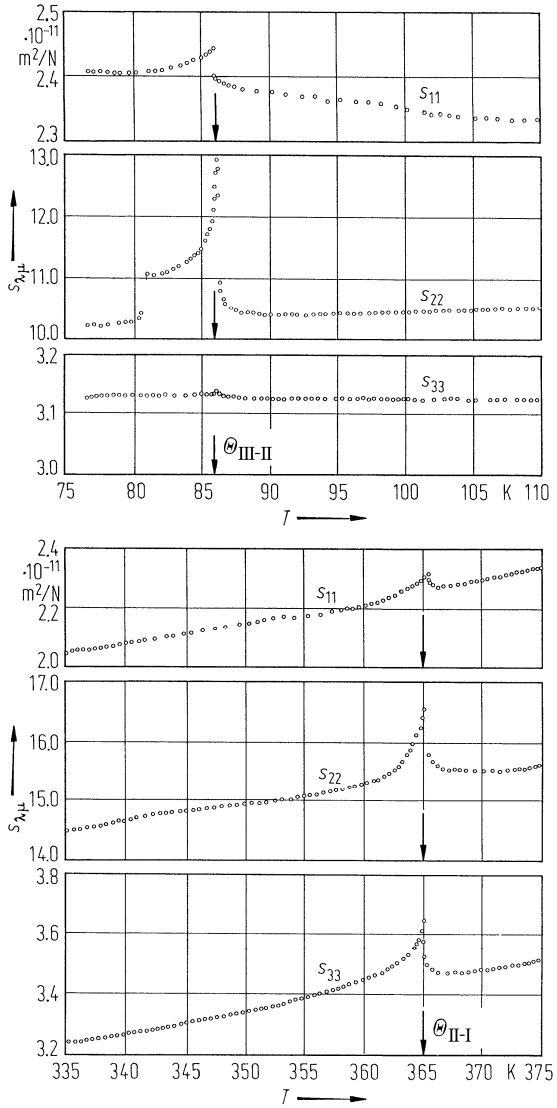

Fig. 65A-1-030. $(CH_3)_3NCH_2COO \cdot H_3PO_4$ (BP). $s_{\lambda\mu}$ vs. T [88Mae]. Composite-bar method.

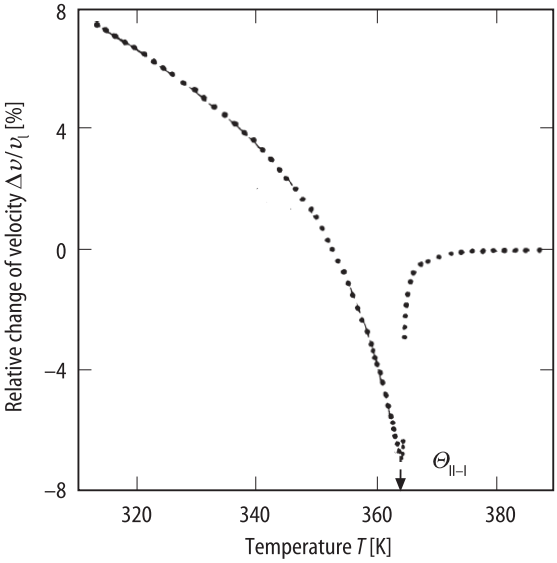

Fig. 65A-1-031. $(CH_3)_3NCH_2COO \cdot (H_{1-x}D_x)_3PO_4$ (DBP). $\Delta v/v_l$ vs. T around Θ_{II-I} [90Alb]. $\Delta v/v_l$: relative change of velocity of longitudinal acoustic wave propagating along [010] direction. f = 15 MHz.

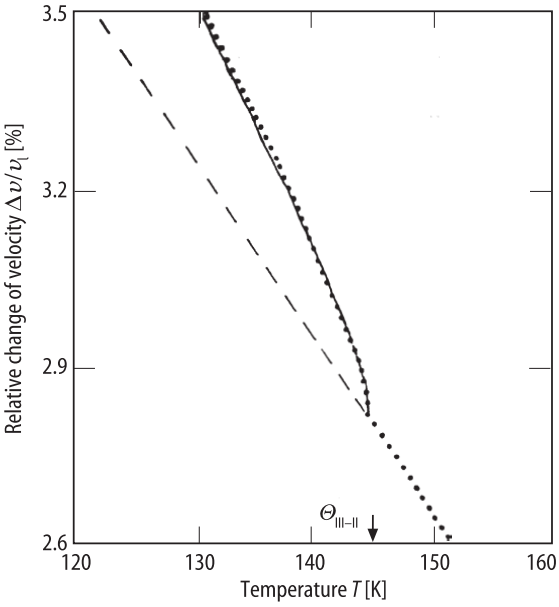

Fig. 65A-1-032. $(CH_3)_3NCH_2COO \cdot (H_{1-x}D_x)_3PO_4$ (DBP). $\Delta v/v_l$ vs. T around Θ_{III-II} [90Alb]. $\Delta v/v_l$: relative change of velocity of longitudinal acoustic wave propagating along [010] direction. f = 15 MHz.

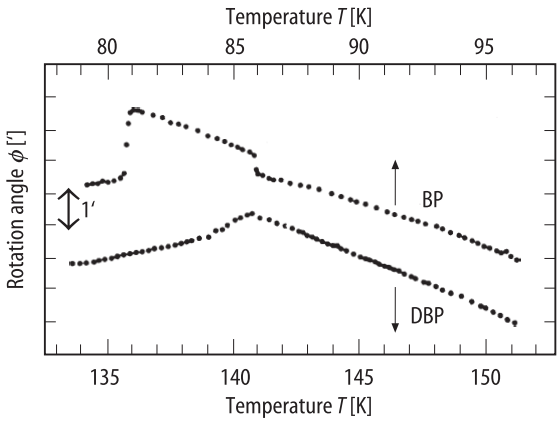

Fig. 65A-1-033. $(CH_3)_3NCH_2COO \cdot H_3PO_4$ (BP), deuterated betaine phosphate (DBP, estimated degree of deuteration: 85 %). ϕ vs. T [90Kro]. ϕ: rotation angle of optical indicatrix. (010) plate. $\lambda = 633$ nm.

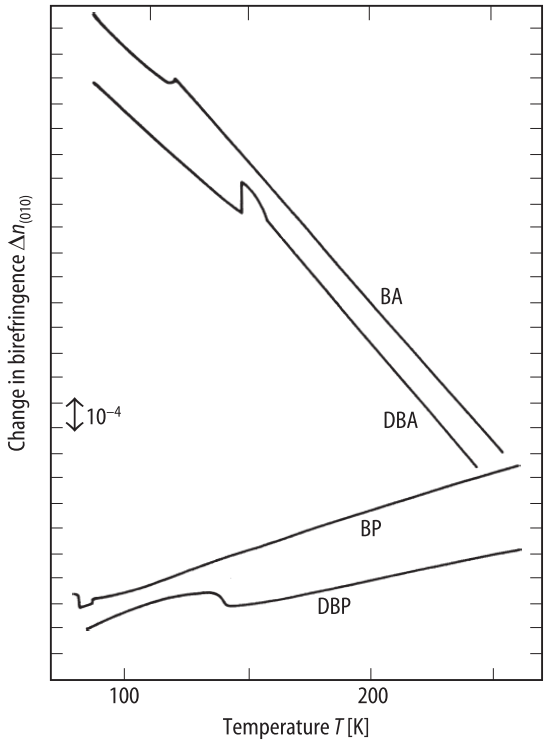

Fig. 65A-1-034. $(CH_3)_3NCH_2COO \cdot H_3PO_4$ (BP), deuterated betaine phosphate (DBP, estimated degree of deuteration: 85 %), $(CH_3)_3NCH_2COO{\cdot}H_3AsO_4$ (BA), deuterated betaine arsenate (DBA, estimated degree of deuteration: 80 %). $\Delta n_{(010)}$ vs. T [90Kro]. $\Delta n_{(010)}$: change in the birefringence measured with (010) plate. $\lambda = 633$ nm.

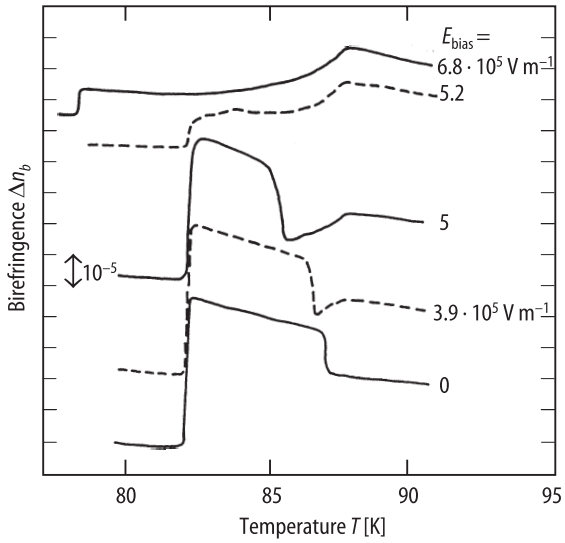

Fig. 65A-1-035. $(CH_3)_3NCH_2COO \cdot H_3PO_4$ (BP). Δn_b vs. T [91Kro]. Parameter: E_{bias} along the b axis. $\lambda = 633$ nm.

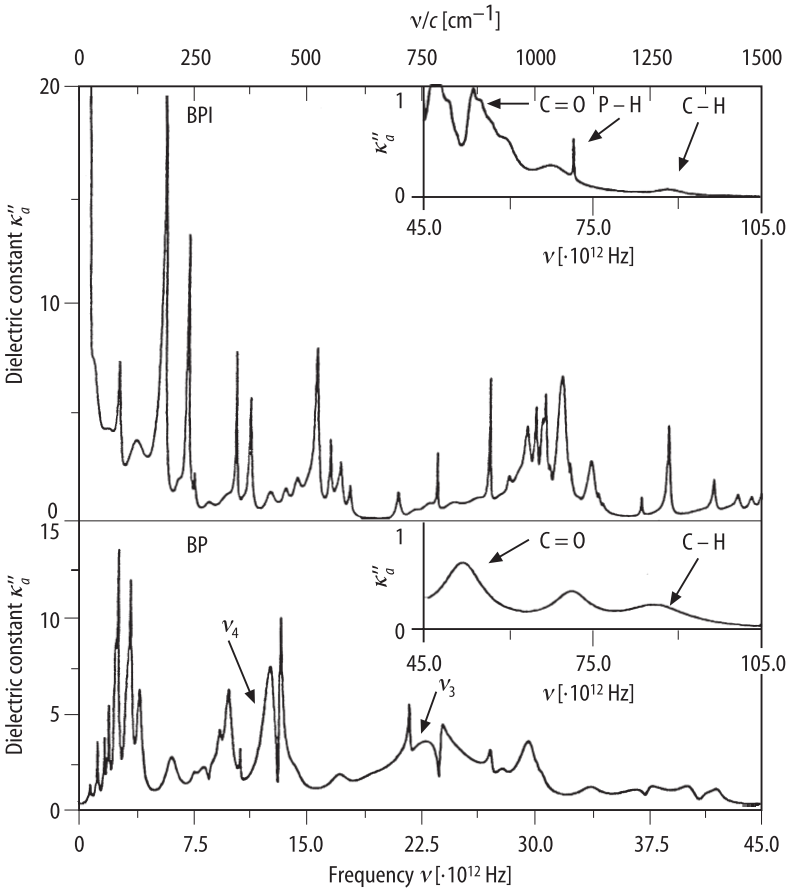

Fig. 65A-1-036. $(CH_3)_3NCH_2COO \cdot H_3PO_4$ (BP), $(CH_3)_3NCH_2COO \cdot H_3PO_3$ (BPI). κ''_a vs. ν [97San]. $T = 4$ K. $\boldsymbol{E} \parallel \boldsymbol{a}$. Obtained from infrared reflectivity data using Kramers-Kronig relation. ν_3 and ν_4 refer to the internal modes of the phosphate tetrahedra, see also Table 65A-1-007.

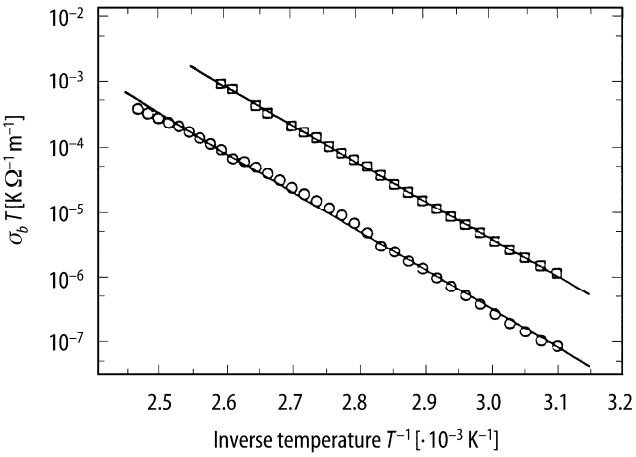

Fig. 65A-1-037. Deuterated betaine phosphate (DBP), deuterated betaine phosphite (DBPI). $\sigma_b T$ vs. T^{-1} [98Fre]. σ_b: DC electrical conductivity along *b* axis. Circle: DBP, square: DBPI. The straight lines are the fits to $\sigma_b = \sigma_0 T^{-1} \exp(-E_A/RT)$, with $\sigma_0 = 4.4 \cdot 10^{11}$ Ω^{-1} m^{-1} and $E_A = 115$ kJ/mol for deuterated betaine phosphate, with $\sigma_0 = 1.2 \cdot 10^{12}$ Ω^{-1} m^{-1} and $E_A = 111$ kJ/mol for deuterated betaine phosphite.

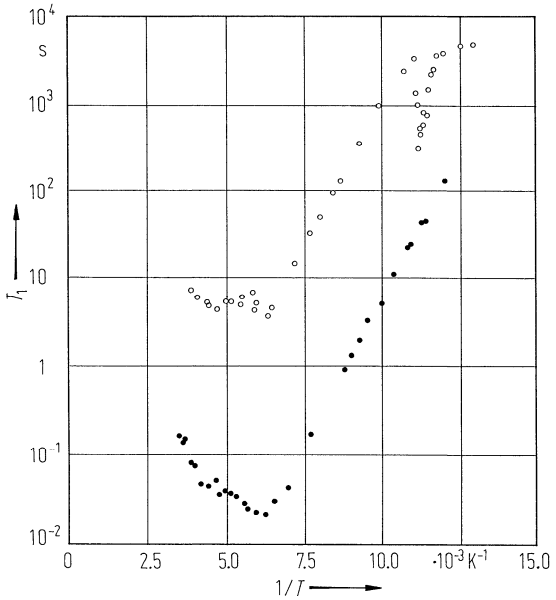

Fig. 65A-1-038. $(CH_3)_3NCH_2COO \cdot H_3PO_4$ (BP). T_1 vs. $1/T$ [87Ohk]. Full circle, open circle: spin-lattice relaxation time of ^{1}H and ^{31}P, respectively.

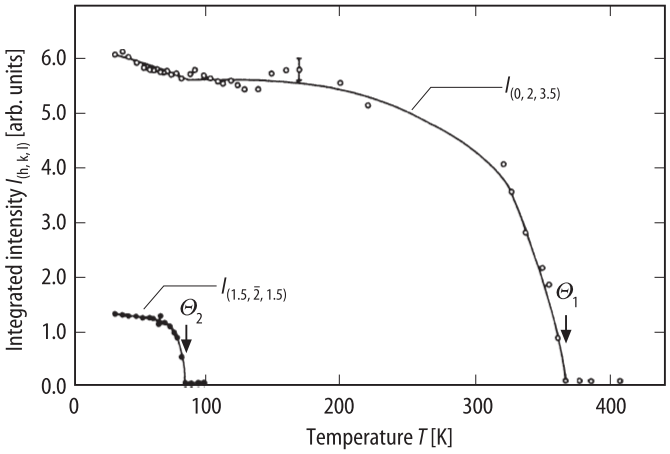

Fig. 65A-1-039. $(CH_3)_3NCH_2COO \cdot H_3PO_4$ (BP). $I_{(h,k,l)}$ vs. T [89Hay]. $I_{(0,\ 2,\ 3.5)}$, $I_{(1.5,\ \bar{2}\ ,\ 1.5)}$: integrated intensity of X-ray superlattice reflections at (0, 2, 3.5) and (1.5, $\bar{2}$, 1.5).

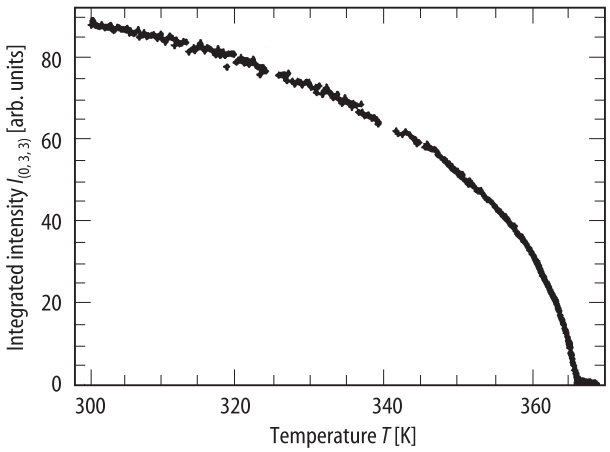

Fig. 65A-1-040. $(CH_3)_3NCH_2COO \cdot H_3PO_4$ (BP). $I_{(0,\ 3,\ 3)}$ vs. T [91Hel]. $I_{(0,\ 3,\ 3)}$: integrated X-ray intensity at (0, 3, 3).

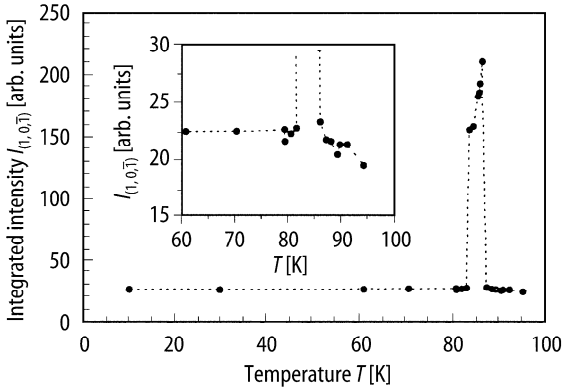

Fig. 65A-1-041. $(CH_3)_3NCH_2COO \cdot H_3PO_4$ (BP). $I_{(1,\ 0,\ \bar{1}\ )}$ vs. T [95San]. $I_{(1,\ 0,\ \bar{1}\ )}$: integrated X-ray intensity at (1, 0, $\bar{1}$).

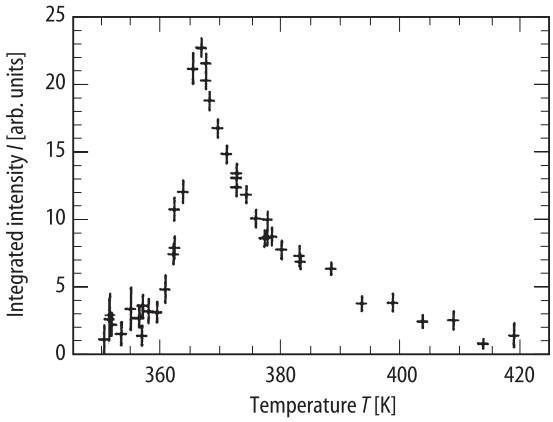

Fig. 65A-1-042. $(CH_3)_3NCH_2COO \cdot H_3PO_4$ (BP). *I* vs. *T* [91Hel]. *I*: integrated intensity of the X-ray critical scattering at (0, 3, 3).

References

82Alb Albers, J., Klöpperpieper, A., Rother, H.J., Ehses, K.H.: Phys. Status Solidi (a) **74** (1982) 553.
84Alb Albers, J., Klöpperpieper, A., Müser, H.E., Rother, H.J.: Ferroelectrics **54** (1984) 45.
84Sch Schildkamp, W., Spilker, J.: Z. Kristallogr. **168** (1984) 159.
85Fre Freitag, O., Brückner, H.J., Unruh, H.-G.: Z. Phys. B **61** (1985) 75.
87Ohk Ohki, H., Nakamura, N., Chihara, H.: Ferroelectrics Lett. **8** (1987) 19.
88Bru Brückner, H.J., Unruh, H.-G., Fischer, G., Genzel, L.: Z. Phys. B **71** (1988) 225.
88Mae Maeda, M.: J. Phys. Soc. Jpn. **57** (1988) 3059.
89Har Hara, K., Umeda, H., Ishibashi, Y., Suzuki, I.: J. Phys. Soc. Jpn. **58** (1989) 4215.
89Hau Haussühl, S.: Z. Kristallogr. **188** (1989) 311.
89Hay Hayase, S., Koshida, T., Terauchi, H., Maeda, M., Suzuki, I.: Ferroelectrics **96** (1989) 221.
89Mae Maeda, M., Atake, T., Saito, Y., Terauchi, H.: J. Phys. Soc. Jpn. **58** (1989) 1135.
89Suz Suzuki, I., Ohta, N., Maeda, M.: Ferroelectrics **96** (1989) 225.
90Alb Albers, J., Balashova, E.V., Klöpperpieper, A., Lemanov, V.V., Müser, H.E., Aherman, A.B.: Ferroelectrics **108** (1990) 357.
90Fis Fischer, G., Brückner, H.J., Klöpperpieper, A., Unruh, H.-G.: Z. Phys. B **79** (1990) 301.
90Kro Kroupa, J., Albers, J.: Ferroelectrics **108** (1990) 341.
91Hel Hellenbrand, K.-H., Ehses, K.H., Krane, H.-G.: Z. Kristallogr. **195** (1991) 251.
91Kro Kroupa, J.: Phase Transitions **36** (1991) 209.
92Lau Launer, S., LeMaire, M., Schaack, G., Haussühl, S.: Ferroelectrics **135** (1992) 257.
92Vol Völkel, G., Pöppl, A., Metz, H.: Ferroelectrics **152** (1992) 11.
94Lan Lanceros-Mendez, S., LeMaire, M., Schaack, G., Schmitt-Lewen, M., Wilhelm, C.: Ferroelectrics **157** (1994) 269.
94Yas Yasuda, N., Konda, J.: Phys. Lett. A **185** (1994) 495.
95Fre Freude, P., Michel, D.: Ferroelectrics **165** (1995) 329.
95San Santos, M.L., Kiat, J.M., Almeida, A., Chaves, M.R., Klöpperpieper, A., Albers, J.: Phys. Status Solidi (b) **189** (1995) 371.
96Fre Freude, P., Michel, D.: Phys. Status Solidi (b) **195** (1996) 297.
97San Santos, M.L., Almeida, A., Chaves, M.R., Klöpperpieper, A., Albers, J., Gomes-Moreira, J.A., Gervais, F.: J. Phys. Condens. Matter **9** (1997) 8119.
98Fre Freude, P., Totz, J., Michel, D., Arndt, M.: J. Phys. Codens. Matter **10** (1998) 429.

No. 65A-2 $(CH_3)_3NCH_2COO \cdot H_3AsO_4$, Betaine arsenate (BA)

(M = 259.09 [D: 273.18])

1a Ferroelectricity in $(CH_3)_3NCH_2COO \cdot H_3AsO_4$ was discovered by Klöpperpieper et al. in 1982. 82Klo

b

phase	III	II	I	
state	F	P		
crystal system		monoclinic		
space group		$P2_1/c - C_{2h}^5$		84Sch
Θ [K]	119 [a])	422 [a])		[a]) 82Klo

The transition temperatures in $(CH_3)_3NC(H_{1-y}D_y)_2COO \cdot (H_{1-x}D_x)_3AsO_4$ are very sensitive to x, but not to y. Therefore, partially deuterated crystals are often labeled in literatures only by x, the D-content in the H_3AsO_4 groups: Fig. 65A-2-001.

For highly deuterated betaine arsenate, the antiferroelectric phase (phase II′) is observed in the intermediate temperature range between phase II and phase III. 84Alb

Θ vs. x phase diagram of $(CH_3)_3NC(H_{1-y}D_y)_2COO \cdot (H_{1-x}D_x)_3AsO_4$: Fig. 65A-2-002.

In BA, another phase transition has been suggested at $T \approx 102$ K. 88Mae

See Fig. 65A-2-006, Fig. 65A-2-008 in subsection 5a.

In $(CH_3)_3NC(H_{1-y}D_y)_2COO \cdot (H_{1-x}D_x)_3AsO_4$ (x = 0.85), another ferroelectric phase has been reported below ≈ 92 K. 94Alm

See Fig. 65A-2-013, Fig. 65A-2-014 in subsection 5a.

P_s lies in the a–c plane, roughly || to the [001] direction. 82Klo

$\rho = 1.704 \cdot 10^3$ kg m^{-3}, $\rho_X = 1.718 \cdot 10^3$ kg m^{-3} at RT. 84Sch

Colorless. 82Klo

Perfect cleavage plane || (100), imperfect cleavage plane || (001). 82Klo

2a Crystal growth: evaporation method from aqueous solution. Starting materials: $(CH_3)_3NCH_2COO \cdot H_2O$ and As_2O_5. 84Alb

b Crystal form: Fig. 65A-2-003, Fig. 65A-2-004.

3a Unit cell parameters: a = 9.556(4) Å, b = 12.897(6) Å, c = 8.128(3) Å, β = 91.23(2)° at RT. 84Sch

Deviation of β from 90°: see Fig. 65A-2-036 in subsection 14a.

b Z = 4 in phase II.

Crystal structure: Fig. 65A-2-005.

Positional and temperature parameters in phase II: Table 65A-2-001.

Interatomic distances and bond angles in phase II: Table 65A-2-002.

5a Low frequency dielectric constant of BA: Fig. 65A-2-006, Fig. 65A-2-007, Fig. 65A-2-008, Fig. 65A-2-009.

Low frequency dielectric constant of $(CH_3)_3NC(H_{1-y}D_y)_2COO \cdot (H_{1-x}D_x)_3AsO_4$: Fig. 65A-2-010, Fig. 65A-2-011, Fig. 65A-2-012, Fig. 65A-2-013, Fig. 65A-2-014.

Curie-Weiss behavior: $\kappa_{(001)} = C/(T - \Theta_{III-II})$, $\Theta_{III-II} < T < \Theta_{III-II} + 8$ K, where $C = 4 \cdot 10^4$ K. 82Klo

See also 87Sch

Dielectric dispersion in BA: Fig. 65A-2-015, Fig. 65A-2-016.

Dielectric dispersion in $(CH_3)_3NC(H_{1-y}D_y)_2COO \cdot (H_{1-x}D_x)_3AsO_4$: Fig. 65A-2-017, Fig. 65A-2-018, Fig. 65A-2-019, Fig. 65A-2-020.

Phase diagram of $(CH_3)_3NC(H_{1-y}D_y)_2COO \cdot (H_{1-x}D_x)_3AsO_4$ in regard to E_{bias}: Fig. 65A-2-021, Fig. 65A-2-022; see also 89Bru

	Phase diagram in regard to p: Fig. 65A-2-023. $d\Theta_{III-II}/dp = -0.045$ K MPa^{-1}.	94Lan
b	Nonlinear dielectric properties: $E = (1/\chi_p)P + \xi P^3 + \zeta P^5 + \eta P^7$, where $\xi = 5.2 \cdot 10^{10}$ V m^5 C^{-3}, $\zeta = 5.2 \cdot 10^{12}$ V m^9 C^{-5}, $\eta = 1.2 \cdot 10^{17}$ V m^{13} C^{-7}. See also Effect of E_{bias} on κ_c' vs. T: Fig. 65A-2-024.	84Mus 84Fru
c	Spontaneous polarization and sublattice polarization: Fig. 65A-2-025, Fig. 65A-2-026, Fig. 65A-2-027; see also Fig. 65A-2-029 and Coercive field and critical field: Fig. 65A-2-028.	87Sch
d	Pyroelectric coefficient: Fig. 65A-2-029; see also	90Alm, 94Alm
6a	Heat capacity near Θ_{III-II}: Fig. 65A-2-030.	
8a	Elastic stiffness and compliance: Table 65A-2-003; Fig. 65A-2-031; see also Sound velocity: Fig. 65A-2-032; see also	85Kru 92Alb, 95Bal
9a	Principal refractive indices: $n_\alpha = 1.498(1)$, $n_\beta = 1.523(1)$ (|| to [010]), $n_\gamma = 1.562(1)$ for $\lambda = 589$ nm at 293 K; see also Fig. 65A-2-004 in subsection 2b. Optical axial angle: $2V = 80.0°$ for $\lambda = 589$ nm at 293 K. Birefringence: Fig. 65A-2-033; see Fig. 65A-1-034 in No. 65A-1; see also Rotation of optical indicatrix: Fig. 65A-2-034, Fig. 65A-2-035.	82Klo 82Klo 91Kro
10a	Raman scattering: see	85Fre, 88Bru
13a	ESR of γ-irradiated crystal: see ^{14}N ENDOR: see	92Vol 93Pop
14a	Bragg reflections: Fig. 65A-2-036.	
16	Twin structure in phase II: see Fig. 65A-2-004 in subsection 2b; see also	88Mae

Table 65A-2-001. $(CH_3)_3NCH_2COO \cdot H_3AsO_4$ (BA). Crystal structure of phase II [84Sch]. Fractional coordinates and temperature parameters [Å^2]. Anisotropic temperature parameters U_{ij} are defined by Eq. (d) in Introduction. T = RT.

	x	y	z	U_{11}	U_{22}	U_{33}	U_{12}	U_{13}	U_{23}
As	0.84579(2)	0.48063(2)	0.243515(3)	0.0275(2)	0.0330(3)	0.0284(2)	0.0030(1)	0.0001(1)	–0.0009(1)
O(3)	0.7088(2)	0.4046(2)	0.2856(3)	0.040(1)	0.040(2)	0.077(1)	0.001(1)	0.010(1)	0.016(1)
O(4)	0.9805(3)	0.4531(2)	0.3681(2)	0.055(1)	0.062(2)	0.046(1)	0.027(1)	–0.023(1)	–0.012(1)
O(5)	0.8020(2)	0.6063(2)	0.2714(2)	0.031(1)	0.034(2)	0.059(1)	0.0038(8)	–0.0033(8)	–0.0009(8)
O(6)	0.8886(2)	0.4601(2)	0.0493(2)	0.043(1)	0.062(2)	0.033(1)	–0.009(1)	0.0026(9)	–0.0122(8)
O(1)	0.5397(2)	0.6473(2)	0.2507(3)	0.026(1)	0.036(2)	0.125(2)	–0.0003(9)	0.001(1)	0.010(1)
O(2)	0.4692(2)	0.4831(2)	0.2727(4)	0.039(1)	0.028(2)	0.125(2)	0.000(1)	0.006(1)	0.003(1)
C(5)	0.4497(2)	0.5790(3)	0.2653(3)	0.027(1)	0.041(3)	0.048(1)	–0.002(1)	–0.004(1)	0.000(1)
C(4)	0.2956(2)	0.6070(2)	0.2790(3)	0.026(1)	0.036(2)	0.037(1)	–0.003(1)	–0.002(1)	–0.001(1)
N	0.2553(2)	0.7186(2)	0.2671(2)	0.028(1)	0.025(2)	0.031(1)	–0.0027(8)	–0.0008(7)	0.0007(8)
C(1)	0.0980(3)	0.7222(3)	0.2830(5)	0.031(1)	0.039(3)	0.083(2)	0.004(1)	0.011(1)	0.008(1)
C(2)	0.2892(3)	0.7644(3)	0.1038(3)	0.049(2)	0.050(2)	0.034(1)	–0.010(1)	0.010(1)	0.009(1)
C(3)	0.3202(4)	0.7824(3)	0.4026(4)	0.072(2)	0.036(3)	0.042(2)		–0.010(1)	–0.012(1)
H(1)	0.080(3)	0.694(3)	0.386(4)	0.07(1)					
H(2)	0.059(4)	0.677(3)	0.194(4)	0.10(1)					
H(3)	0.084(3)	0.798(3)	0.288(3)	0.07(1)					
H(4)	0.241(3)	0.831(3)	0.099(3)	0.07(1)					
H(5)	0.247(3)	0.718(3)	0.026(4)	0.07(1)					
H(6)	0.389(3)	0.765(2)	0.092(3)	0.054(7)					
H(7)	0.282(3)	0.855(3)	0.388(3)	0.07(1)					
H(8)	0.431(3)	0.776(2)	0.386(3)	0.060(8)					
H(9)	0.301(3)	0.749(3)	0.504(3)	0.08(1)					
H(10)	0.272(2)	0.588(2)	0.380(3)	0.048(7)					
H(11)	0.248(3)	0.567(2)	0.192(3)	0.052(7)					
H(12)	0.6513(3)	0.424(4)	0.256(4)	0.073(8)					
H(13)	0.982(9)	0.465(7)	0.430(9)	U(H12)					
H(14)	0.722(3)	0.615(3)	0.263(4)	U(H12)					
H(15)	0.943(7)	0.468(6)	0.06(1)	U(H12)					

Table 65A-2-002. $(CH_3)_3NCH_2COO \cdot H_3AsO_4$ (BA). Crystal structure of phase II [84Sch]. Interatomic distances and bond angles. T = RT.

Distance [Å]		Angle [°]	
As–O(3)	1.695(2)	O(3)–As–O(4)	110.4(1)
As–O(4)	1.675(2)	O(4)–As–O(5)	108.3(1)
As–O(5)	1.704(2)	O(5)–As–O(6)	110.3(1)
As–O(6)	1.679(2)	O(6)–As–O(4)	110.0(1)
C(5)–O(1)	1.249(4)	O(1)–C(5)–O(2)	127.2(2)
C(5)–O(2)	1.260(4)	O(2)–C(5)–C(4)	111.9(2)
C(5)–C(4)	1.537(3)	O(1)–C(5)–C(4)	120.8(3)
C(4)–N	1.501(4)	C(5)–C(4)–N	118.2(2)
C(3)–N	1.518(4)	C(3)–N–C(4)	112.3(2)
C(2)–N	1.512(3)	C(2)–N–C(4)	112.2(2)
C(1)–N	1.528(3)	C(1)–N–C(4)	106.3(2)
C(1)–H(1)	0.93(3)	C(1)–N–C(2)	107.4(2)
C(1)–H(2)	1.00(4)	C(1)–N–C(3)	108.5(2)
C(1)–H(3)	0.98(4)	N–C(1)–H(3)	100(2)
C(2)–H(4)	0.97(4)	C(2)–N–C(3)	109.9(2)
C(2)–H(5)	0.95(3)	N–C(2)–H(5)	104(2)
C(2)–H(6)	0.96(3)	N–C(2)–H(6)	109(2)
C(3)–H(7)	1.01(4)	N–C(3)–H(7)	107(2)
C(3)–H(8)	1.07(3)	N–C(3)–H(8)	105(2)
C(3)–H(9)	0.95(3)	N–C(3)–H(9)	108(2)
C(4)–H(10)	0.89(3)	N–C(4)–H(10)	105(2)
C(4)–H(11)	0.98(3)	N–C(4)–H(11)	110(2)
O(3)–H(12)	0.61(3)	As–O(4)–H(13)	121(9)
O(4)–H(13)	0.52(8)	As–O(3)–H(12)	117(4)
O(5)–H(14)	0.77(3)	As–O(5)–H(14)	112(3)
O(6)–H(15)	0.53(7)	As–O(6)–H(15)	93(9)
O(2)–O(3)	2.501(3)	O(2)–H(12)–O(3)	174(5)
O(1)–O(5)	2.565(3)	O(1)–H(14)–O(5)	174(4)
O(4)–O(4)	2.485(6)	O(4)–H(13)–O(4)	161(12)
O(6)–O(6)	2.516(5)	O(6)–H(15)–O(6)	148(8)
H(13)–H(13)	1.53(16)	As–O(4)–O(4)	121.5(2)
H(15)–H(15)	1.58(12)	As–O(6)–O(6)	117.8(2)

Table 65A-2-003. $(CH_3)_3NCH_2COO \cdot H_3AsO_4$ (BA), $(CH_3)_3NCH_2COO \cdot H_3PO_4$ (BP). Elastic stiffness constants $c_{\lambda\mu}$ [$\cdot 10^{10}$ N m^{-2}] [85Kru]. Obtained from Brillouin scattering.

$c_{\lambda\mu}$	BA	BP	$c_{\lambda\mu}$	BA	BP
c_{11}	2.11(1)	2.98(6)	c_{12}	0.90(1)	1.0(1)
c_{22}	1.52(1)	1.93(2)	c_{13}	0.76(1)	1.12(1)
c_{33}	1.85(1)	1.35(1)	c_{33}	0.76(1)	0.82(1)
c_{44}	0.64(1)	0.63(1)	c_{15}	0.06(1)	–0.56(6)
c_{55}	0.36(1)	0.38(3)	c_{25}	–0.07(10)	–0.31(8)
c_{66}	0.67(1)	0.27(1)	c_{35}	0.01(1)	–0.20(1)
			c_{46}	0.06(1)	0.09(2)

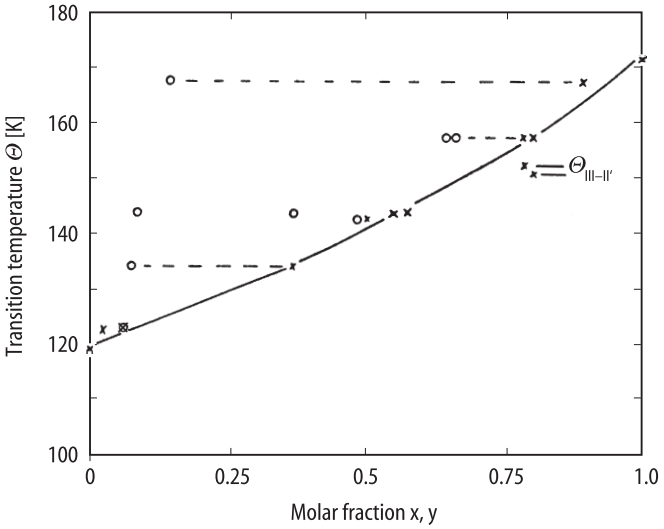

Fig. 65A-2-001. $(CH_3)_3NC(H_{1-y}D_y)_2COO \cdot (H_{1-x}D_x)_3AsO_4$. Θ vs. x, y [85Rot]. Crosses: Θ vs. x, open circles: Θ vs. y. Dashed lines connect data of the same samples.

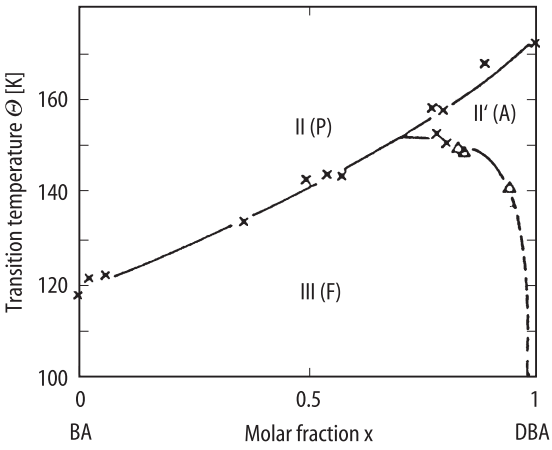

Fig. 65A-2-002. $(CH_3)_3NC(H_{1-y}D_y)_2COO \cdot (H_{1-x}D_x)_3AsO_4$. Θ vs. x [90Sch]. x: degree of deuteration of the H-bonds between the betaine-molecule and the arsenate-group. For y, see subsection 1b. Phase II′: antiferroelectric phase.

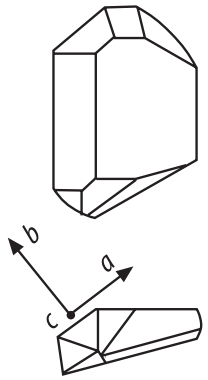

Fig. 65A-2-003. $(CH_3)_3NCH_2COO \cdot H_3AsO_4$ (BA). Typical crystal form [88Mae].

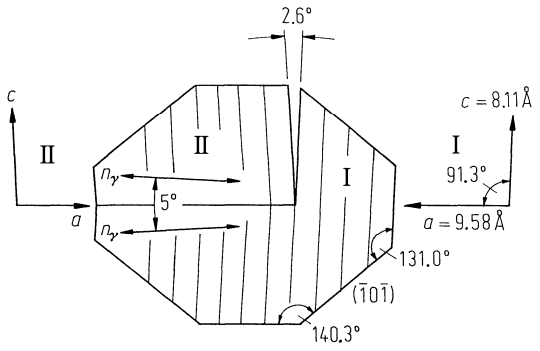

Fig. 65A-2-004. $(CH_3)_3NCH_2COO \cdot H_3AsO_4$ (BA). Crystal form and the crystallographic directions [82Klo]. I and II indicate the two different domains of twin structure. The (100) lattice planes (thin lines) and the direction of optical extinction are shown. The deviations from an orthorhombic system are shown enlarged for clarity.

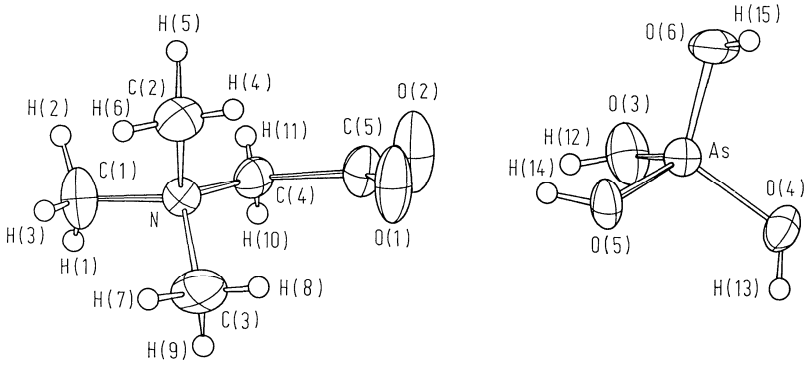

Fig. 65A-2-005. $(CH_3)_3NCH_2COO \cdot H_3AsO_4$ (BA). Structure of one formula unit at RT [84Sch]. Anisotropic temperature parameters are illustrated.

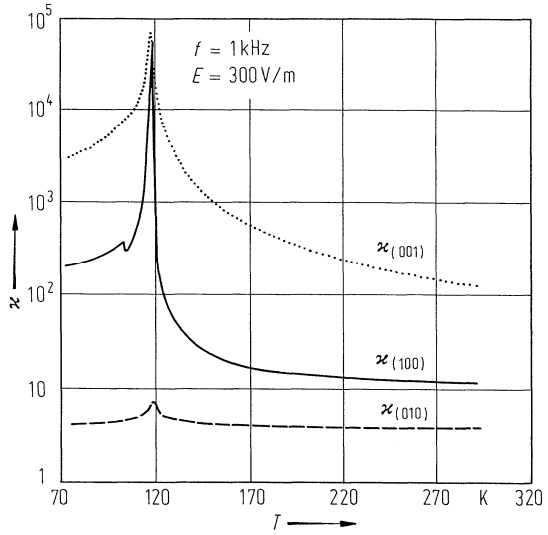

Fig. 65A-2-006. $(CH_3)_3NCH_2COO \cdot H_3AsO_4$ (BA). $\varkappa_{(100)}$, $\varkappa_{(010)}$, $\varkappa_{(001)}$ vs. T [82Klo]. f = 1 kHz.

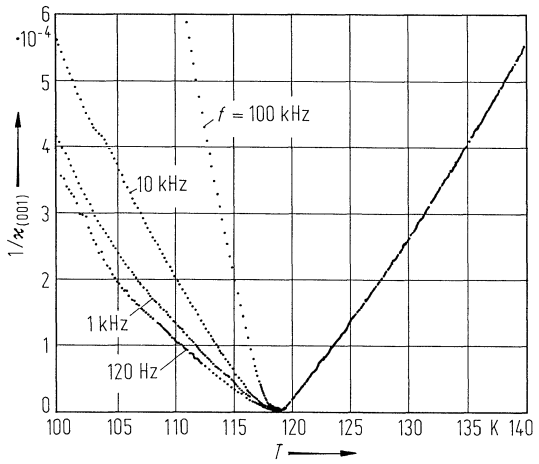

Fig. 65A-2-007. $(CH_3)_3NCH_2COO \cdot H_3AsO_4$ (BA). $1/\varkappa_{(001)}$ vs. T [84Mus]. Parameter: f.

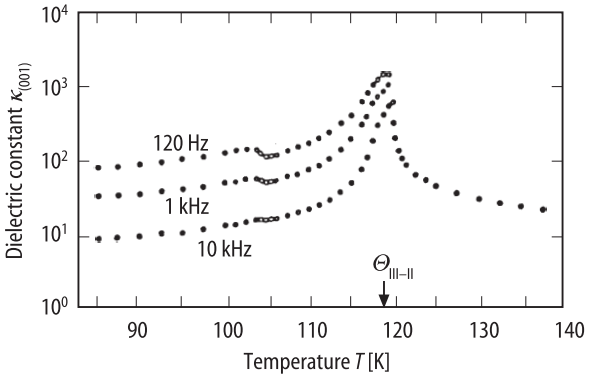

Fig. 65A-2-008. $(CH_3)_3NCH_2COO \cdot H_3AsO_4$ (BA). $\varkappa_{(001)}$ vs. T [89Suz]. Parameter: f.

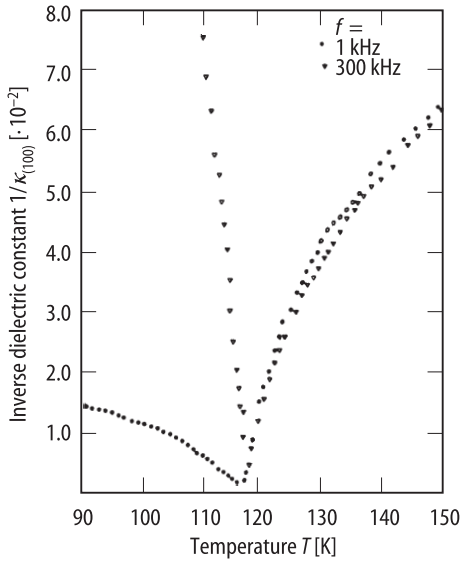

Fig. 65A-2-009. $(CH_3)_3NCH_2COO \cdot H_3AsO_4$ (BA). $1/\varkappa_{(100)}$ vs. T [88Mae]. Parameter: f.

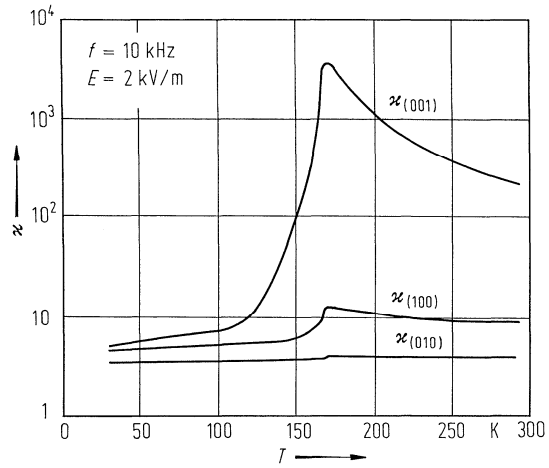

Fig. 65A-2-010. $(CH_3)_3NCH_2COO \cdot (H_{1-x}D_x)_3AsO_4$ (x = 0.99). $\varkappa_{(100)}$, $\varkappa_{(010)}$, $\varkappa_{(001)}$ vs. T [84Alb]. f = 10 kHz.

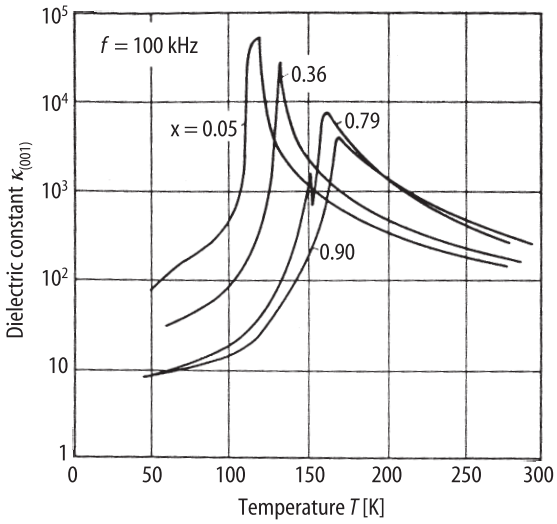

Fig. 65A-2-011. $(CH_3)_3NC(H_{1-y}D_y)_2COO \cdot (H_{1-x}D_x)_3AsO_4$. $\varkappa_{(001)}$ vs. T [85Rot]. Parameter: x. For y, see subsection 1b.

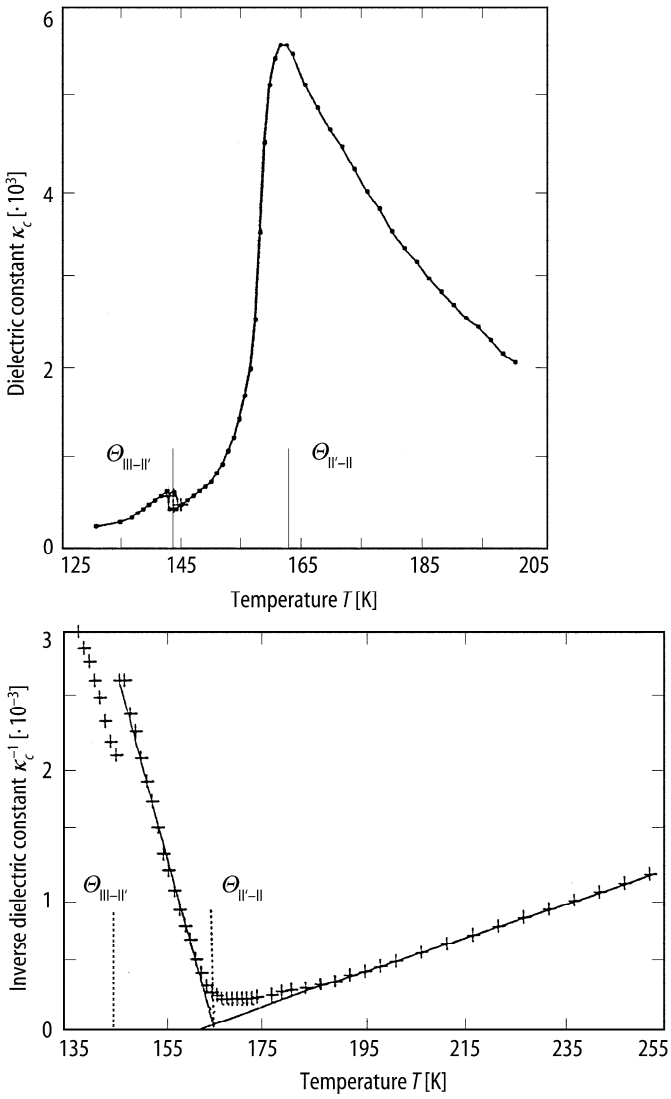

Fig. 65A-2-012. $(CH_3)_3NC(H_{1-y}D_y)_2COO \cdot (H_{1-x}D_x)_3AsO_4$ (x = 0.85, for y, see subsection 1b). κ_c, $1/\kappa_c$ vs. T [95Bal]. f = 1 kHz.

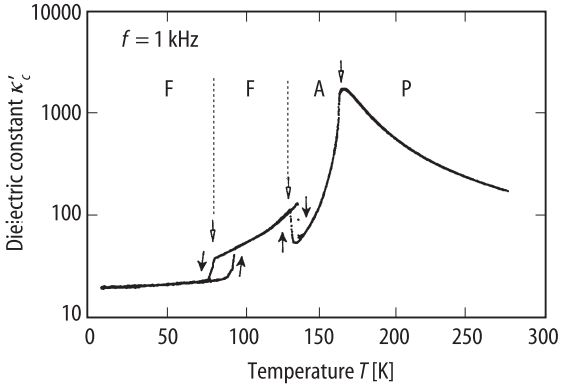

Fig. 65A-2-013. $(CH_3)_3NC(H_{1-y}D_y)_2COO \cdot (H_{1-x}D_x)_3AsO_4$ (x = 0.85, for y, see subsection 1b). κ_c' vs. T [94Alm]. P, A, F denote paraelectric, antiferroelectric, and ferroelectric phases, respectively.

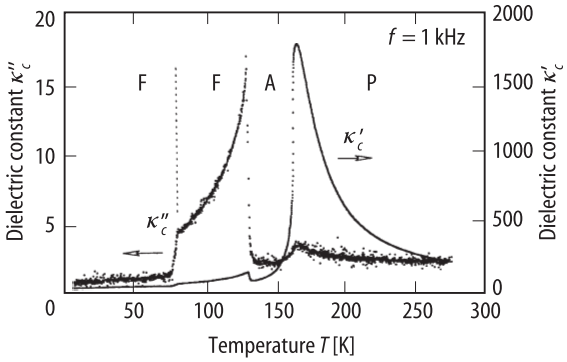

Fig. 65A-2-014. $(CH_3)_3NC(H_{1-y}D_y)_2COO \cdot (H_{1-x}D_x)_3AsO_4$ (x = 0.85, for y, see subsection 1b). κ_c', κ_c'' vs. T [94Alm]. P, A, F denote paraelectric, antiferroelectric, and ferroelectric phases, respectively.

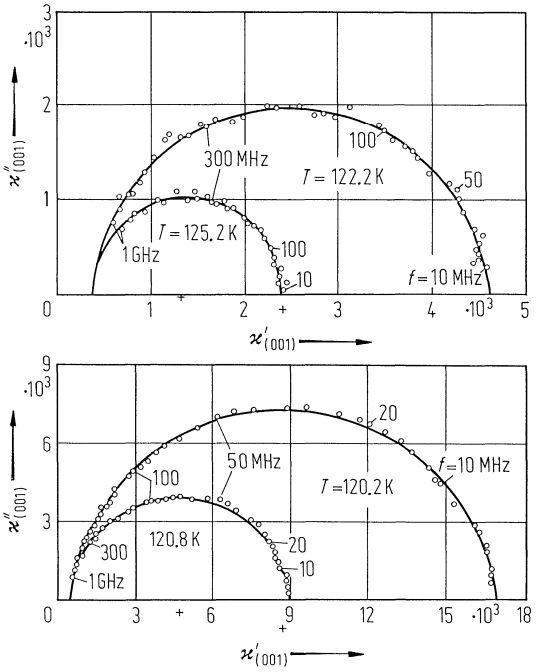

Fig. 65A-2-015. $(CH_3)_3NCH_2COO \cdot H_3AsO_4$ (BA). Cole-Cole plot of the complex dielectric constant [85Fre]. Parameter: T. Measured for a (001) plate.

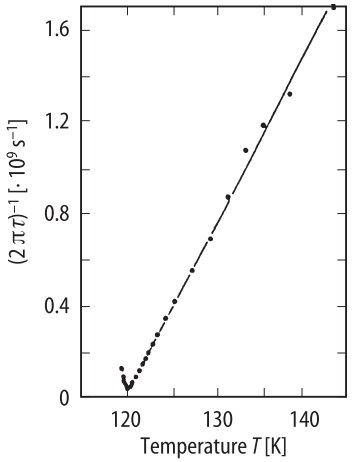

Fig. 65A-2-016. $(CH_3)_3NCH_2COO \cdot H_3AsO_4$ (BA). $(2\pi\tau)^{-1}$ vs. T [85Fre]. τ: dielectric relaxation time.

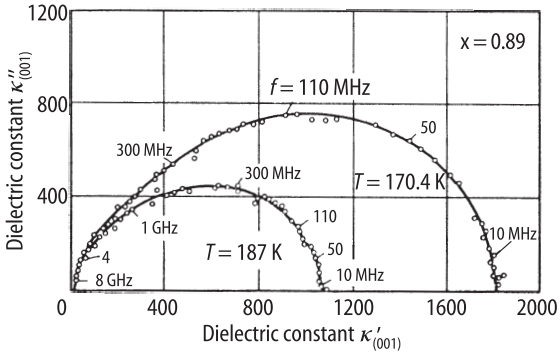

Fig. 65A-2-017. $(CH_3)_3NC(H_{1-y}D_y)_2COO \cdot (H_{1-x}D_x)_3AsO_4$ (x = 0.89, for y, see subsection 1b). Cole-Cole plot of the complex dielectric constant [85Fre]. Measured for a (001) plate.

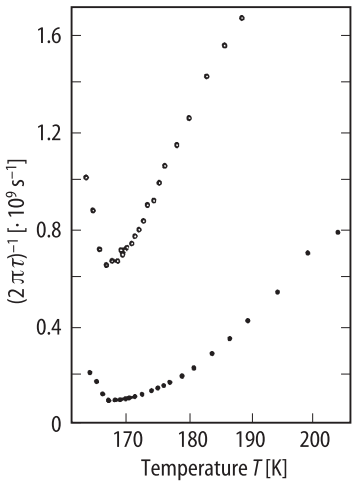

Fig. 65A-2-018. $(CH_3)_3NC(H_{1-y}D_y)_2COO \cdot (H_{1-x}D_x)_3AsO_4$ (x = 0.89, for y, see subsection 1b). $(2\pi\tau)^{-1}$ vs. T [85Fre]. τ: dielectric relaxation time. Two dielectric relaxations have been reported.

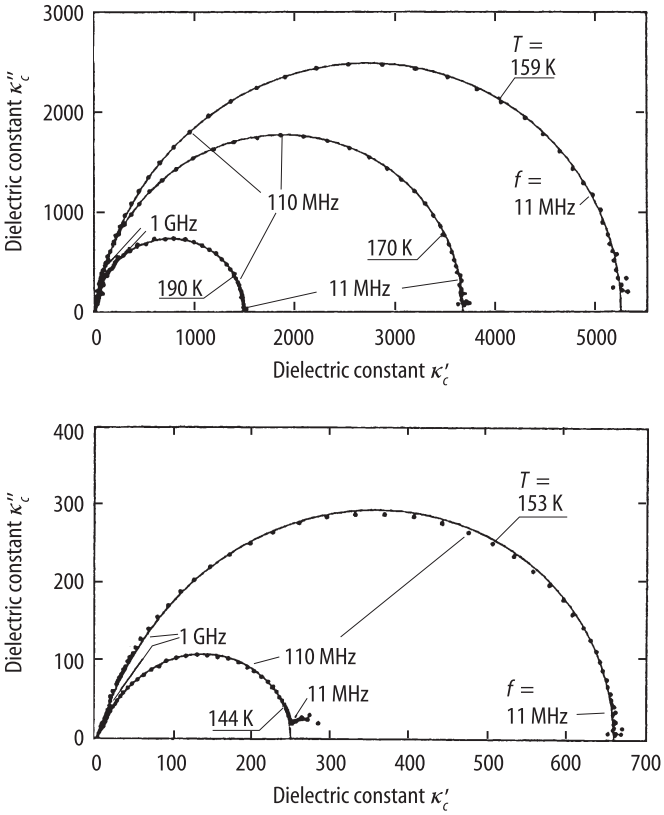

Fig. 65A-2-019. $(CH_3)_3NC(H_{1-y}D_y)_2COO \cdot (H_{1-x}D_x)_3AsO_4$ (x = 0.80, for y, see subsection 1b). Cole-Cole diagram of the complex dielectric constant [89Bru]. Parameter: *T*. The lines are the Cole-Davidson fits.

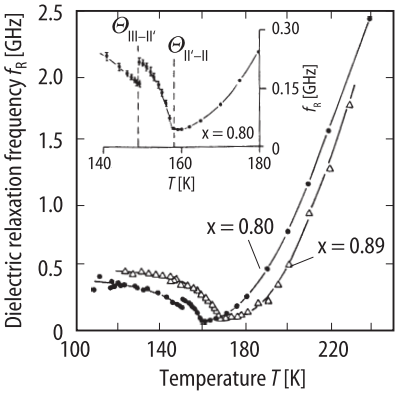

Fig. 65A-2-020. $(CH_3)_3NC(H_{1-y}D_y)_2COO \cdot (H_{1-x}D_x)_3AsO_4$. f_R vs. *T* [89Bru]. Parameter: x. For y, see subsection 1b. f_R: dielectric relaxation frequency (the frequency of the maximum of κ'').

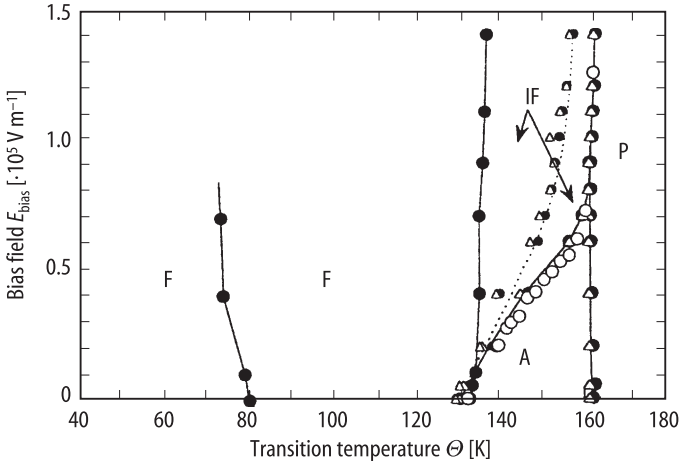

Fig. 65A-2-021. $(CH_3)_3NC(H_{1-y}D_y)_2COO \cdot (H_{1-x}D_x)_3AsO_4$ (x = 0.85, for y, see subsection 1b). E_{bias} vs. Θ [94Alm]. P, A, IF, F denote paraelectric, antiferroelectric, induced-ferroelectric and ferroelectric phases, respectively. Full circle: dielectric constant measurements, open triangle: pyroelectric measurements, open circle: $D - E$ hysteresis loop measurements.

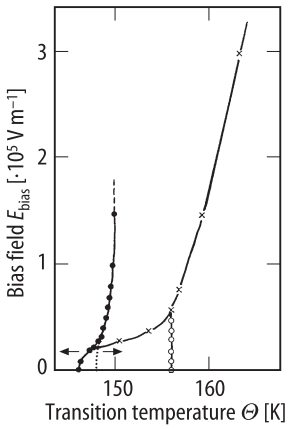

Fig. 65A-2-022. $(CH_3)_3NC(H_{1-y}D_y)_2COO \cdot (H_{1-x}D_x)_3AsO_4$ (x = 0.80, for y, see subsection 1b). E_{bias} vs. Θ phase diagram [91Kro]. Obtained from birefringence measurements. Dotted line in the figure indicates the result on heating.

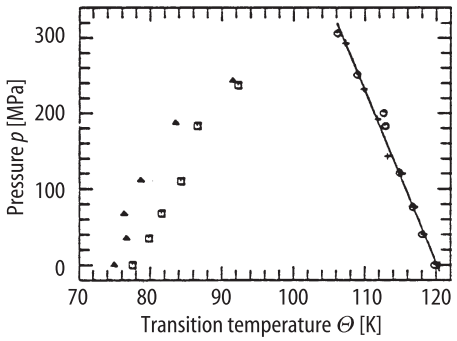

Fig. 65A-2-023. $(CH_3)_3NCH_2COO \cdot H_3AsO_4$ (BA). p vs. Θ [92Lau]. Open circle, full triangle: coefficient of drift of temperature $dT/dt < 0$, plus, square: $dT/dt > 0$. Points around 80 K show broad dielectric peaks.

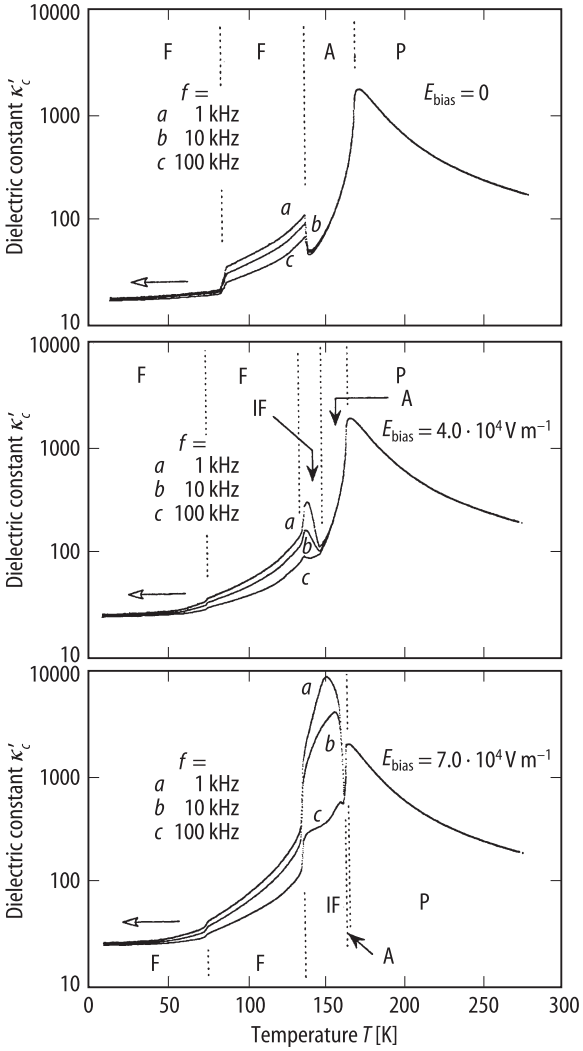

Fig. 65A-2-024. $(CH_3)_3NC(H_{1-y}D_y)_2COO \cdot (H_{1-x}D_x)_3AsO_4$ (x = 0.85, for y, see subsection 1b). κ_c' vs. T at various E_{bias} [94Alm]. Parameter: *f*. P, A, F denote paraelectric, antiferroelectric, and ferroelectric phases, respectively. IF denotes the ferroelectric phase induced by E_{bias}.

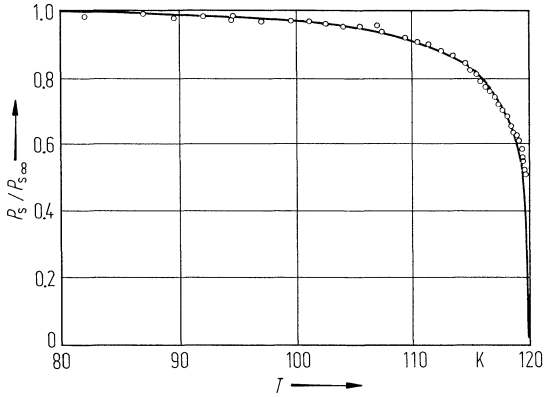

Fig. 65A-2-025. $(CH_3)_3NCH_2COO \cdot H_3AsO_4$ (BA). $P_s/P_{s\infty}$ vs. T [84Mus]. $P_{s\infty}$: saturated spontaneous polarization ($= 3.2 \cdot 10^{-2}$ C m^{-2}).

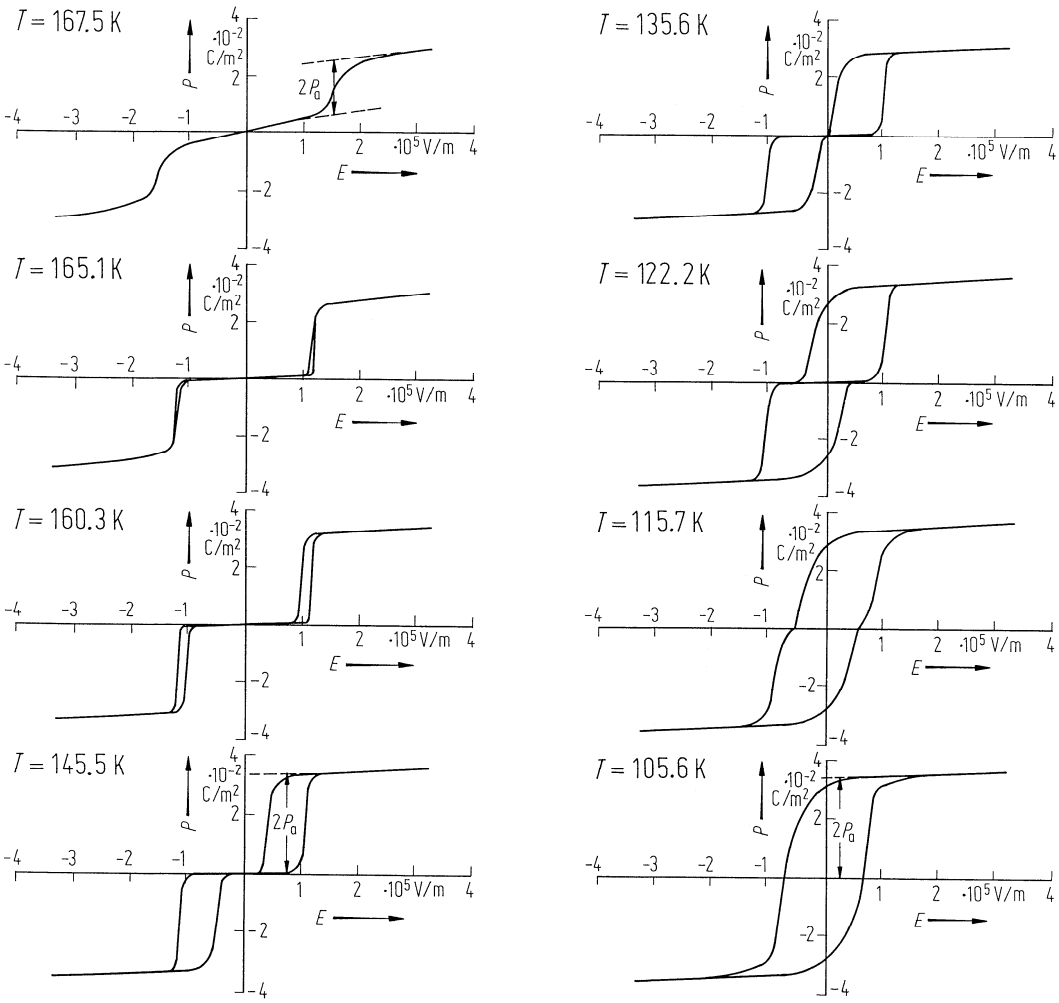

Fig. 65A-2-026. $(CH_3)_3NCH_2COO \cdot (H_{1-x}D_x)_3AsO_4$ (x = 0.99). *P* vs. *E* [84Alb]. Parameter: *T*. *f* = 1 Hz. Measured for (001) plate.

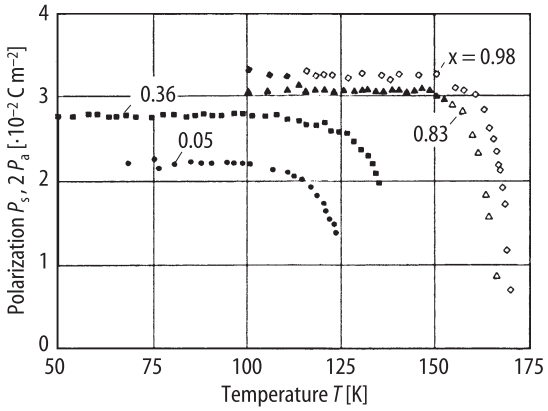

Fig. 65A-2-027. $(CH_3)_3NC(H_{1-y}D_y)_2COO \cdot (H_{1-x}D_x)_3AsO_4$. P_s, $2P_a$ vs. *T* [85Rot]. Parameter: x. For y, see subsection 1b. P_a: sublattice polarization. Open symbols and full symbols indicate $2P_a$ and P_s, respectively.

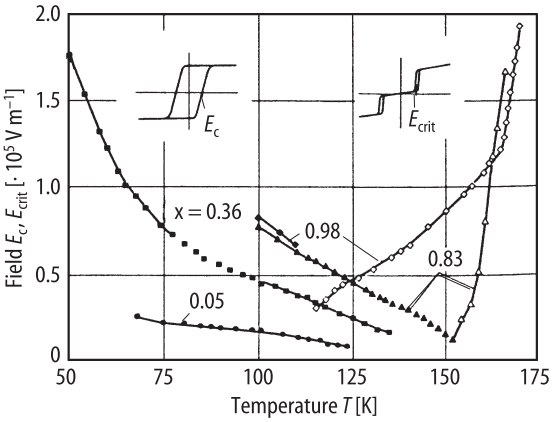

Fig. 65A-2-028. $(CH_3)_3NC(H_{1-y}D_y)_2COO \cdot (H_{1-x}D_x)_3AsO_4$. E_c, E_{crit} vs. T [85Rot]. Parameter: x. For y, see subsection 1b. E_{crit}: critical field of antiferroelectric $D - E$ hysteresis loop. See the inserts. Open symbols and closed symbols indicate E_{crit} and E_c, respectively.

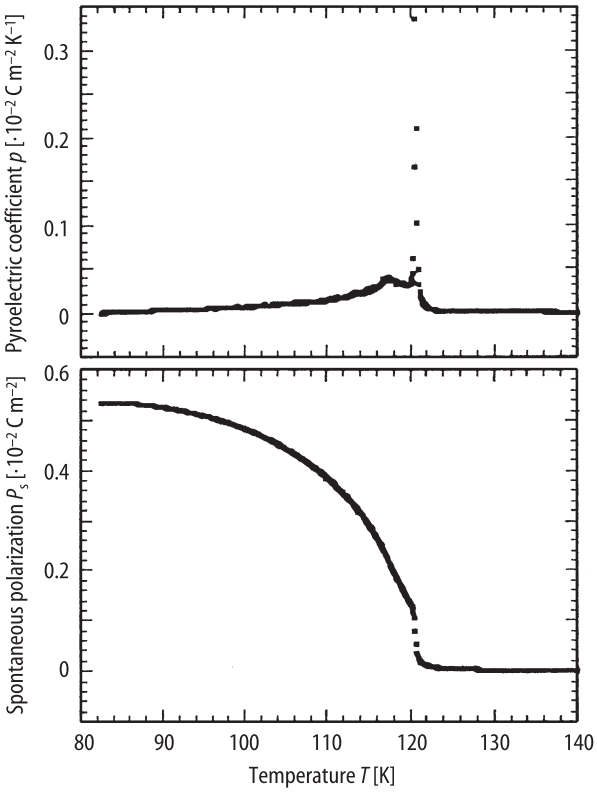

Fig. 65A-2-029. $(CH_3)_3NCH_2COO \cdot H_3AsO_4$ (BA). p, P_s vs. T [94Lac]. p: pyroelectric coefficient along the c axis.

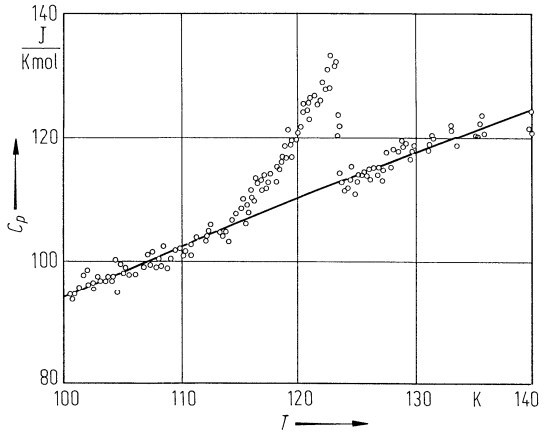

Fig. 65A-2-030. $(CH_3)_3NCH_2COO \cdot H_3AsO_4$ (BA). C_p vs. T near Θ_{III-II} [84Fru]. C_p: molar heat capacity at constant pressure.

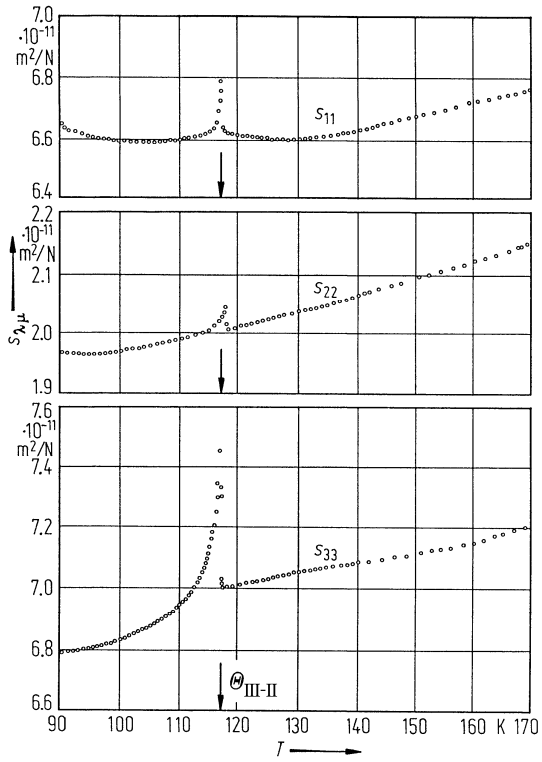

Fig. 65A-2-031. $(CH_3)_3NCH_2COO \cdot H_3AsO_4$ (BA). $s_{\lambda\mu}$ vs. T [88Mae]. Composite-bar method.

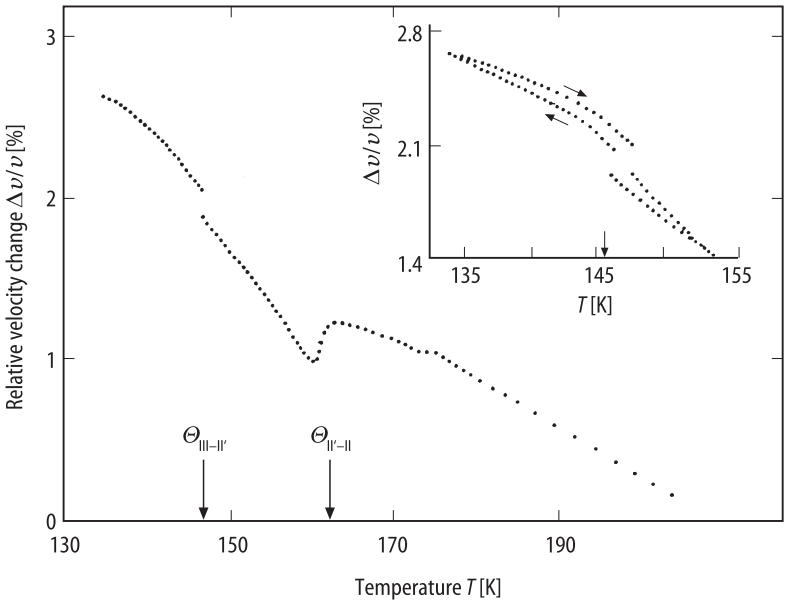

Fig. 65A-2-032. $(CH_3)_3NC(H_{1-y}D_y)_2COO \cdot (H_{1-x}D_x)_3AsO_4$ (x = 0.85, for y, see subsection 1b). $\Delta v/v$ vs. T [91Alb]. $\Delta v/v$: relative change in the velocity for a longitudinal acoustic wave propagating along c axis. f = 15 MHz.

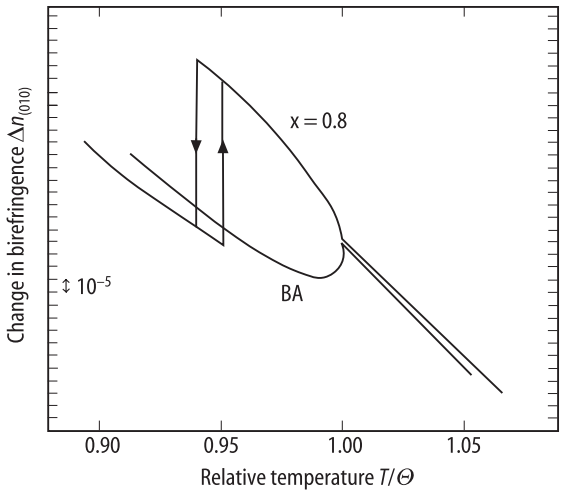

Fig. 65A-2-033. $(CH_3)_3NCH_2COO \cdot H_3AsO_4$ (BA), $(CH_3)_3NC(H_{1-y}D_y)_2COO \cdot (H_{1-x}D_x)_3AsO_4$ (x = 0.8, for y, see subsection 1b). $\Delta n_{(010)}$ vs. T/Θ [90Kro]. $\Delta n_{(010)}$: change in the birefringence measured for (010) plate. λ = 633 nm. $\Theta = \Theta_{III-II}$ (= 119.1 K) for BA, $\Theta = \Theta_{II'-II}$ (= 156 K) for deuterated BA with x = 0.8.

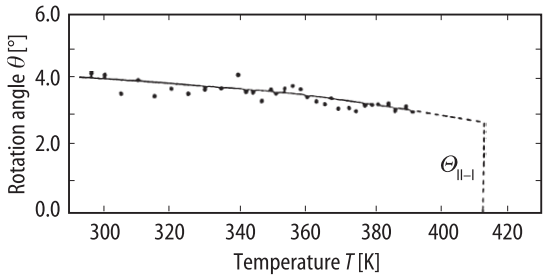

Fig. 65A-2-034. $(CH_3)_3NCH_2COO \cdot H_3AsO_4$ (BA). θ vs. T [88Mae]. θ: rotation angle of indicatrix about b axis.

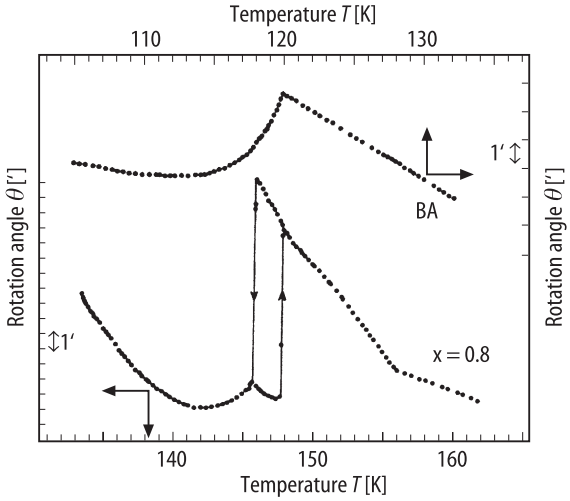

Fig. 65A-2-035. $(CH_3)_3NCH_2COO \cdot H_3AsO_4$ (BA), $(CH_3)_3NC(H_{1-y}D_y)_2COO \cdot (H_{1-x}D_x)_3AsO_4$ (x = 0.8, for y, see subsection 1b). θ vs. T [90Kro]. θ: rotation angle of indicatrix. Measured for (010) plate. λ = 633 nm.

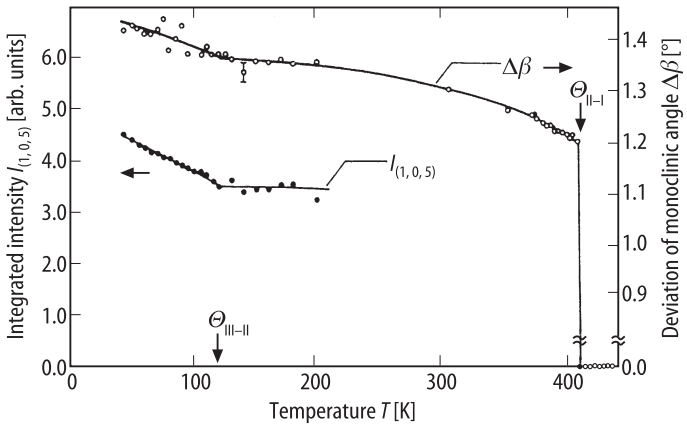

Fig. 65A-2-036. $(CH_3)_3NCH_2COO \cdot H_3AsO_4$ (BA). $I_{(1, 0, 5)}$, $\Delta\beta$ vs. T [89Hay]. $I_{(1, 0, 5)}$: integrated intensity of X-ray Bragg reflection at (1, 0, 5). $\Delta\beta$: deviation of monoclinic angle β from 90°.

References

82Klo Klöpperpieper, A., Rother, H.J., Albers, J., Ehses, K.H.: Ferroelectrics Lett. **44** (1982) 115.
84Alb Albers, J., Klöpperpieper, A., Müser, H.E., Rother, H.J.: Ferroelectrics **54** (1984) 45.
84Fru Frühauf, K.-P, Sauerland, E., Helwig, J., Müser, H.E.: Ferroelectrics **54** (1984) 293.
84Mus Müser, H.E., Schell, U.: Ferroelectrics **55** (1984) 279.
84Sch Schildkamp, W., Schäfer, G., Spilker, J.: Z. Kristallogr. **168** (1984) 187.
85Fre Freitag, O., Bruckner, H.J., Unruh, H.-G.: Z. Phys. B **61** (1985) 75.
85Kru Krüger, J.K., Peetz, L., Albers, J., Müser, H.E.: Ferroelectrics Lett. **4** (1985) 111.
85Rot Rother, H.J., Albers, J., Klöpperpieper, A., Müser, H.E.: Jpn. J. Appl. Phys. **24** (1985) Suppl. 24–2, 384.
87Sch Schell, U., Müser, H.E.: Z. Phys. B **66** (1987) 237.
88Bru Brückner, H.J., Unruh, H.-G., Fischer, G., Genzel, L.: Z. Phys. B **71** (1988) 225.
88Mae Maeda, M.: J. Phys. Soc. Jpn. **57** (1988) 2162.
89Bru Brückner, H.J.: Z. Phys. B **75** (1989) 259.
89Hay Hayase, S., Koshida, T., Terauchi, K., Maeda, M., Suzuki, I.: Ferroelectrics **96** (1989) 221.
89Suz Suzuki, I., Ohta, N., Maeda, M.: Ferroelectrics **96** (1989) 225.
90Alm Almeida, A., Carvalho, P.S., Chaves, M.R., Pires, A.R., Müser, H.E., Klöpperpieper, A.: Ferroelectrics **108** (1990) 347.
90Kro Kroupa, J., Albers, J.: Ferroelectrics **108** (1990) 341.
90Sch Schaack, G.: Ferroelectrics **104** (1990) 147.
91Alb Albers, J., Balashova, E.V., Klöpperpieper, A., Lemanov, V.V., Müser, H.E., Sherman A.B.: Fiz. Tverd. Tela **33** (1991)2363; Sov. Phys. Solid State (English Transl.) **33** (1991) 1330.
91Kro Kroupa, J.: Phase Transitions **36** (1991) 209.
92Alb Albers, J., Balashova, E.V., Klöpperpieper, A. Lemanov, V.V., Müser, H.E., Sherman, A.B.: Ferroelectrics **125** (1992) 93.
92Lau Launer, S., LeMaire, M., Schaack, G., Haussühl, S.: Ferroelectrics **135** (1992) 257.
92Vol Völkel, G., Pöppl, A., Metz, H., Klöpperpieper, A.: Ferroelectrics **125** (1992) 11.
93Pop Pöppl, A., Völkel, G.: Chem. Phys. **171** (1993) 387.
94Alm Almeida, A., Carvalho, P.S., Chaves, M.R., Klöpperpieper, A., Albers, J.: Phys. Status Solidi (b) **184** (1994) 225.
94Lac Lacerda-Aroso, M.T., Ribeiro, J.L., Chaves, M.R., Almeida, A., Vieira, L.G., Klöpperpieper, A., Albers, J.: Phys. Status Solidi (b) **185** (1994) 265.
94Lan Lanceros-Mendez, S., LeMaire, M., Schaack, G., Schmitt-Lewen, M., Wilhelm, C.: Ferroelectrics **157** (1994) 269.
95Bal Balashova, E.V., Lemanov, V.V., Tagantsev, A.K., Sherman, A.B., Shomuradov, Sh.H.: Phys. Rev. B **51** (1995) 8747.

No. 65A-3 $(CH_3)_3NCH_2COO \cdot H_3PO_3$, Betaine phosphite (BPI)

(M = 199.14 [D: 213.23])

1a Ferroelectricity in $(CH_3)_3NCH_2COO \cdot H_3PO_3$ was discovered by Albers et al. in 1988. 88Alb1, 88Alb2

b

phase	III	II	I	
state	F	P	P	
crystal system	monoclinic	monoclinic	monoclinic	
space group	$P2_1 - C_2^2$	$P2_1/c - C_{2h}^5$	$P2_1/m - C_{2h}^2$	[a]) 88Alb1
Θ [K]	206···224 [a]) [D: 298 [c])		355 354.4 [b])]	[b]) 96Fre [c]) 96Ban

$\rho = 1.381 \cdot 10^3$ kg m^{-3}, $\rho_X = 1.382 \cdot 10^3$ kg m^{-3}. 88Alb1
Colorless. 88Alb1
Cleavage plane || $(10\bar{2})$; see Fig. 65A-3-018 in subsection 9a. 88Alb1

2a Crystal growth: evaporation method from aqueous solution containing betaine and H_3PO_3 in the molar ratio 1:1. 88Alb1

3a Unit cell parameters: a = 11.191(3) Å, b = 7.591(3) Å, c = 12.447(6) Å, β = 116.62(2)° at RT. 89Dor
See Fig. 65B-2-003 in No. 65B-2; see also 93Feh

b Z = 4 in phase II.
Crystal structure of phase II: Table 65A-3-001; Fig. 65A-3-001; see also 89Dor

4 Thermal expansion coefficients at RT: see Table 65A-1-005 in No. 65A-1.

5a Curie-Weiss constant: $C = 2.1 \cdot 10^4$ K. 93Sob
Low frequency dielectric constant: Fig. 65A-3-002, Fig. 65A-3-003, Fig. 65A-3-004, Fig. 65A-3-005.
Dielectric dipserson in BPI: Fig. 65A-3-006, Fig. 65A-3-007, Fig. 65A-3-008.
Dielectric dipserson in DBPI: Fig. 65A-3-009, Fig. 65A-3-010.
Effect of p on κ: Fig. 65A-3-011;
$[d\Theta_{II-II}/dp]_{p=0} = -0.122$ K MPa^{-1}. 95Ebe
See also 92Lau
Phase diagram in regard to p: Fig. 65A-3-012; see also 95Ebe

b Nonlinear dielectric properties: $E = (1/\chi_p)P + \xi P^3 + \zeta P^5$, where $\xi = 2.71 \cdot 10^{11}$ V m^5 C^{-3}, $\zeta = 2.3 \cdot 10^{14}$ V m^9 C^{-5}. 95Cac

c Spontaneous polarization and coercive field:
Fig. 65A-3-013, Fig. 65A-3-014, Fig. 65A-3-015.

6a Heat capacity: Fig. 65A-3-016, Fig. 65A-3-017.
Transition entropy: $\Delta S_{II-I} = 2.2$ J mol^{-1} K^{-1}. 88Alb1

8a Elastic stiffness and bulk compressibility: see Table 65A-1-006 in No. 65A-1.

9a Principal refractive indices: n_α = 1.478(2) (|| to [010]), n_β = 1.498(2), n_γ = 1.527(2) for λ = 589 nm at 22 °C; 88Alb1
Fig. 65A-3-018.
Infrared reflection spectra: see 95Ebe, 97San

κ'' obtained from far-infrared reflectivity: see Fig. 65A-1-036 in No. 65A-1.

10a	Raman scattering: see	95Ebe
11	Electrical conductivity: see Fig. 65A-1-037 in No. 65A-1 and also	98Fre
13a	NMR: chemical exchange processes of deuterons; see	98Fre
	^{1}H ENDOR: see	93Bau
b	ESR of γ-irradiated crystal: see	92Vol

Table 65A-3-001. $(CH_3)_3NCH_2COO \cdot H_3PO_3$ (BPI). Fractional coordinates at RT (phase II) [93Feh]. Neutron diffraction. The site occupation of H13 and H15 is 0.5. See Fig. 65A-3-001.

Atom	*x*	*y*	*z*
O1	0.0404(1)	0.2301(3)	0.4169(1)
O2	1.0085(1)	0.2427(4)	0.2273(1)
C5	0.9688(1)	0.2430(2)	0.3105(1)
C4	0.8198(1)	0.2657(2)	0.2555(1)
N	0.75866(9)	0.2639(1)	0.34009(8)
C1	0.6132(1)	0.2910(3)	0.2660(2)
C2	0.7788(2)	0.0911(2)	0.4032(2)
C3	0.8096(2)	0.4104(3)	0.4288(2)
H1	0.5977(4)	0.4161(7)	0.2214(4)
H2	0.5762(3)	0.1885(8)	0.1997(4)
H3	0.5650(3)	0.2860(8)	0.3243(4)
H4	0.7242(5)	0.0923(6)	0.4542(5)
H5	0.7455(6)	–0.0118(6)	0.3373(6)
H6	0.8824(5)	0.0751(6)	0.4627(5)
H7	0.7514(5)	0.4130(6)	0.4786(4)
H8	0.9116(5)	0.3860(6)	0.4896(4)
H9	0.7977(5)	0.5316(6)	0.3826(5)
H10	0.7943(3)	0.3924(5)	0.2090(3)
H11	0.7736(3)	0.1619(5)	0.1903(3)
P	0.3601(1)	0.2539(2)	0.4186(1)
O3	0.2513(1)	0.1980(2)	0.3013(2)
O4	0.4877(2)	0.1486(3)	0.4555(2)
H14	0.3199(3)	0.2268(6)	0.5089(3)
O6	0.3908(2)	0.4485(2)	0.4209(2)
H12	0.1120(3)	0.2284(5)	0.2631(3)
H13	0.503(1)	0.0347(8)	0.497(1)
H15	0.517(2)	0.500(5)	0.518(1)

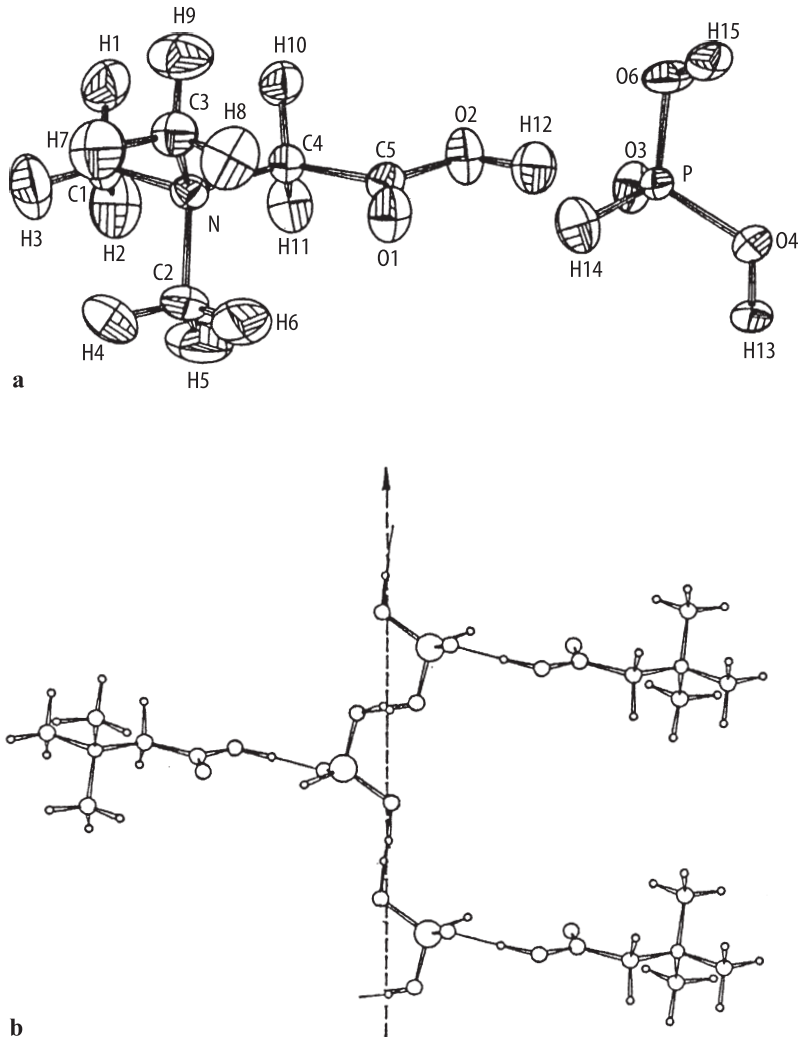

Fig. 65A-3-001. $(CH_3)_3NCH_2COO \cdot H_3PO_3$ (BPI). Crystal structure in phase II [93Feh]. Neutron scattering. $T = 295$ K. (**a**) ORTEP plot of BPI unit. (**b**) Schematic drawing of the BPI units; the dashed line represents the monoclinic *b* axis.

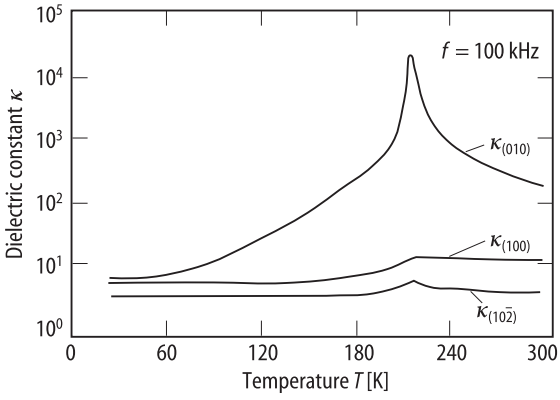

Fig. 65A-3-002. $(CH_3)_3NCH_2COO \cdot H_3PO_3$ (BPI). $\kappa_{(010)}$, $\kappa_{(100)}$, $\kappa_{(10\bar{2})}$ vs. T [88Alb1]. $\kappa_{(hkl)}$: dielectric constant of specimen cut || to (hkl). $f = 100$ kHz.

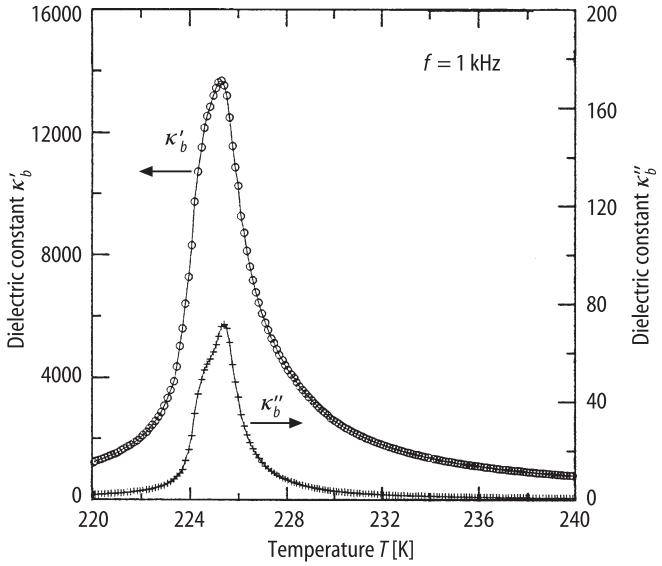

Fig. 65A-3-003. $(CH_3)_3NCH_2COO \cdot H_3PO_3$ (BPI). κ'_b, κ''_b vs. T [95Cac]. f = 1 kHz.

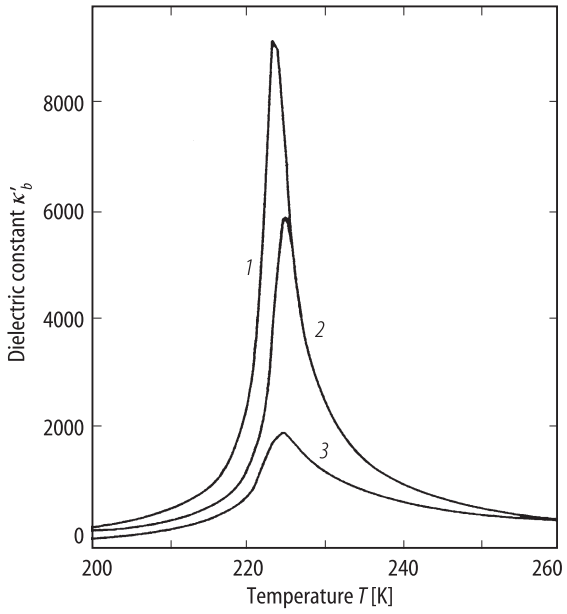

Fig. 65A-3-004. $(CH_3)_3NCH_2COO \cdot H_3PO_3$ (BPI). κ'_b vs. T [93Sob]. Curve *1*: multidomain sample, f = 1 MHz. *2*: single domain sample, f = 1 MHz. *3*: clamped sample, f = 100 MHz.

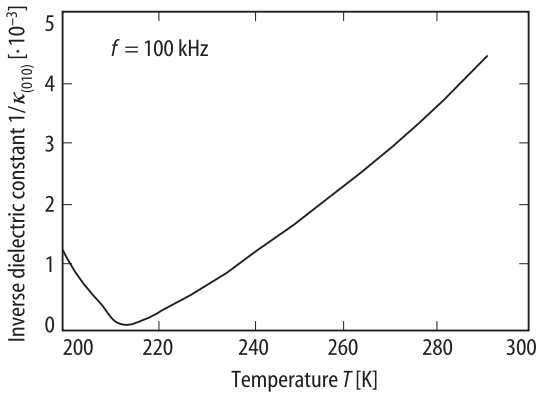

Fig. 65A-3-005. $(CH_3)_3NCH_2COO \cdot H_3PO_3$ (BPI). $1/\kappa_{(010)}$ vs. T [88Alb1]. $\kappa_{(010)}$: dielectric constant of (010) plate. f = 100 kHz.

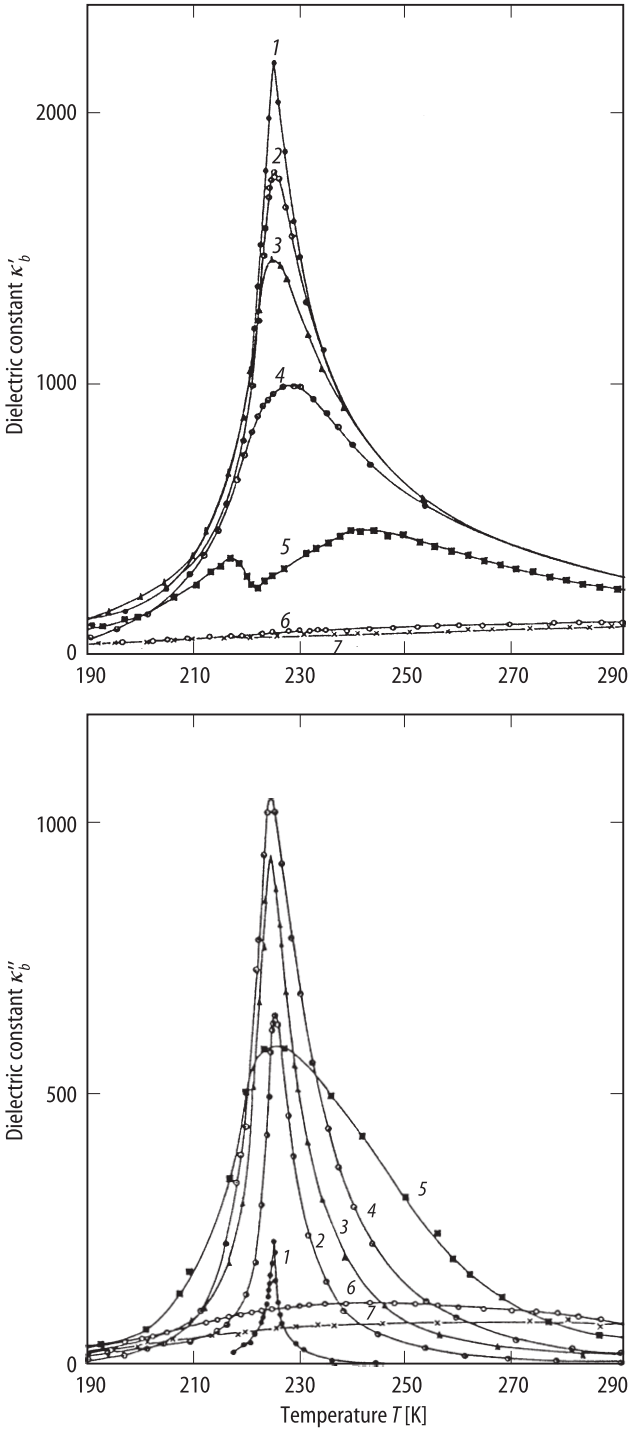

Fig. 65A-3-006. $(CH_3)_3NCH_2COO \cdot H_3PO_3$ (BPI). κ'_b, κ''_b vs. T [93Sob]. Parameter: *f*. Curve *1*: 0.1 GHz, *2*: 1 GHz, *3*: 2 GHz, *4*: 3.8 GHz, *5*: 8.8 GHz, *6*: 54 GHz, *7*: 77 GHz.

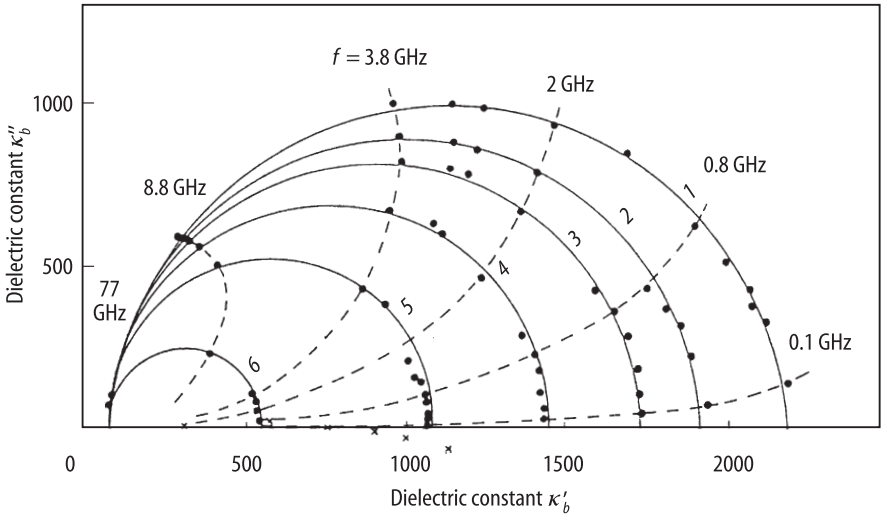

Fig. 65A-3-007. $(CH_3)_3NCH_2COO \cdot H_3PO_3$ (BPI). Cole-Cole diagram of complex dielectric constant [93Sob]. Parameter: $T - \Theta_{III-II}$. Curve *1*: $T - \Theta_{III-II}$ = 1 K, *2*: 2.5 K, *3*: 3.5 K, *4*: 6 K, *5*: 11 K, *6*: 31 K. The crosses near κ_b' axis mark the centers of the semicircles.

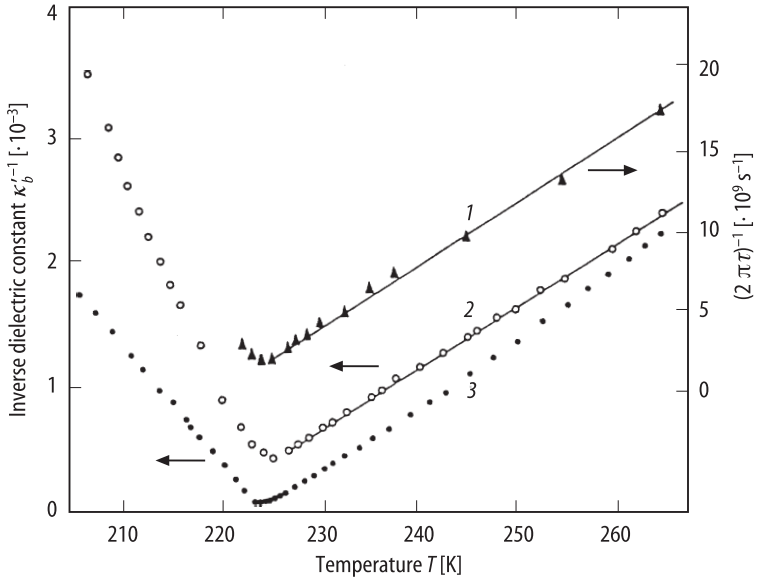

Fig. 65A-3-008. $(CH_3)_3NCH_2COO \cdot H_3PO_3$ (BPI). $\kappa_b'^{-1}$, $(2\pi\tau)^{-1}$ vs. T [93Sob]. Curve *1*: $(2\pi\tau)^{-1}$; τ: dielectric relaxation time. *2*: contribution of the relaxational mode to reciprocal dielectric constant. *3*: $\kappa_b'^{-1}$ of the free crystal.

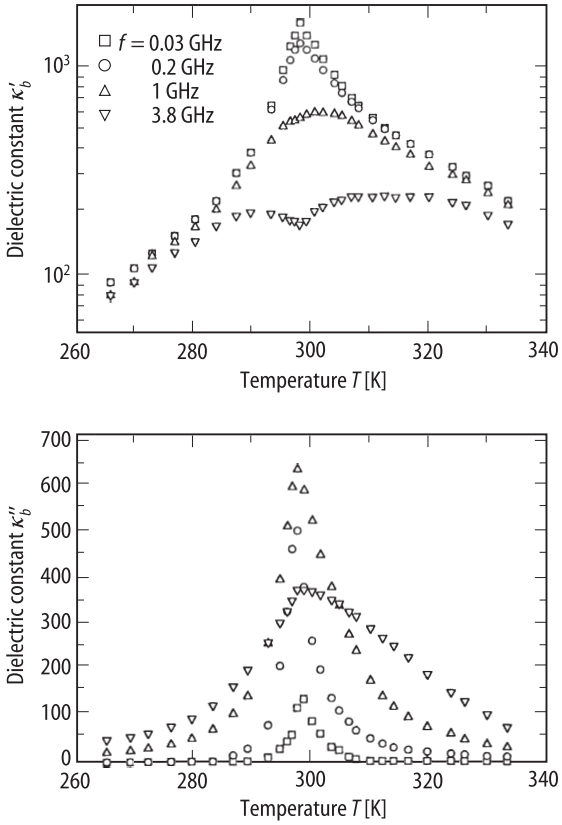

Fig. 65A-3-009. $(CH_3)_3NCH_2COO \cdot D_3PO_3$ (DBPI). κ_b', κ_b'' vs. T [96Ban]. Parameter: f.

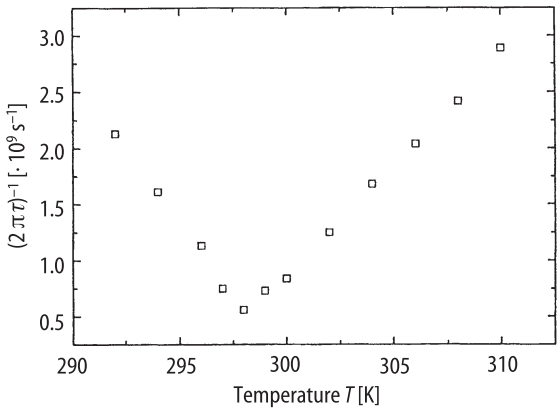

Fig. 65A-3-010. $(CH_3)_3NCH_2COO \cdot D_3PO_3$ (DBPI). $(2\pi\tau)^{-1}$ vs. T [96Ban]. τ: dielectric relaxation time.

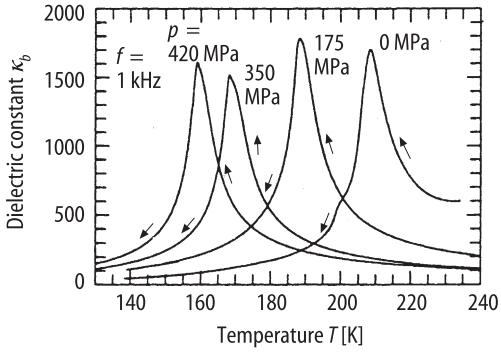

Fig. 65A-3-011. $(CH_3)_3NCH_2COO \cdot H_3PO_3$ (BPI). κ_b vs. T [92Lau]. Parameter: p. f = 1 kHz.

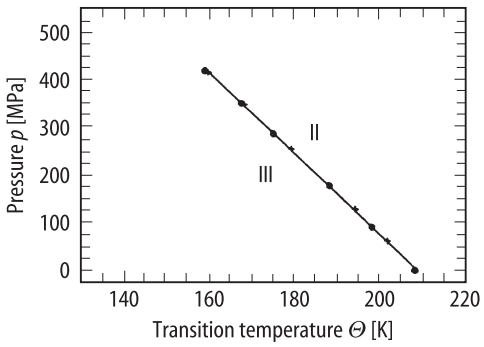

Fig. 65A-3-012. $(CH_3)_3NCH_2COO \cdot H_3PO_3$ (BPI). Θ vs. p [92Lau].

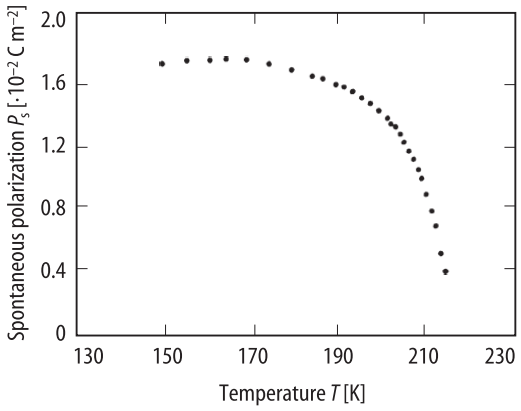

Fig. 65A-3-013. $(CH_3)_3NCH_2COO \cdot H_3PO_3$ (BPI). P_s vs. T [88Alb1]. Dielectric hysteresis loop measurement.

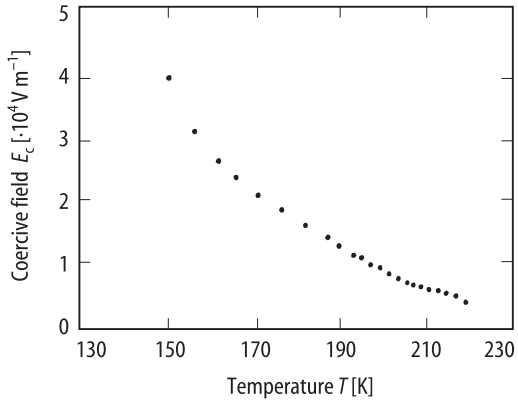

Fig. 65A-3-014. $(CH_3)_3NCH_2COO \cdot H_3PO_3$ (BPI). E_c vs. T [88Alb1]. E_c: coercive electric field.

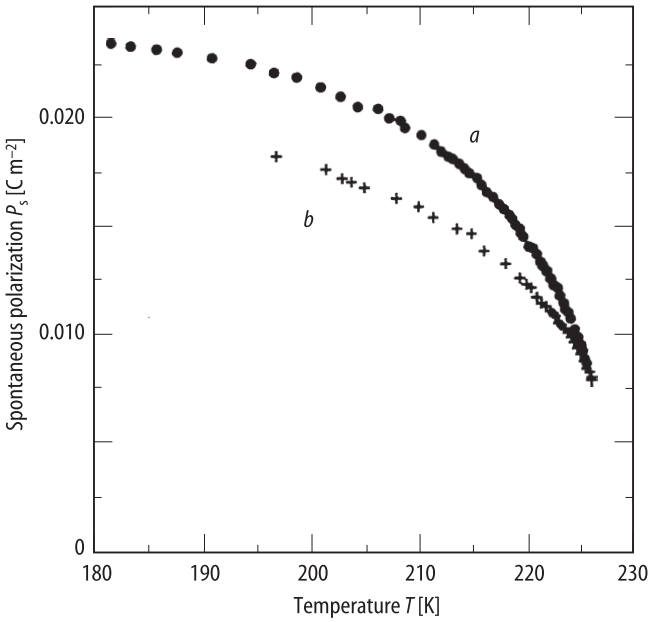

Fig. 65A-3-015. $(CH_3)_3NCH_2COO \cdot H_3PO_3$ (BPI). P_s vs. T [95Cac]. Curve *a*: P_s obtained after several measurement series, *b*: P_s at first cooling to ferroelectric phase. Dielectric hysteresis loop measurement.

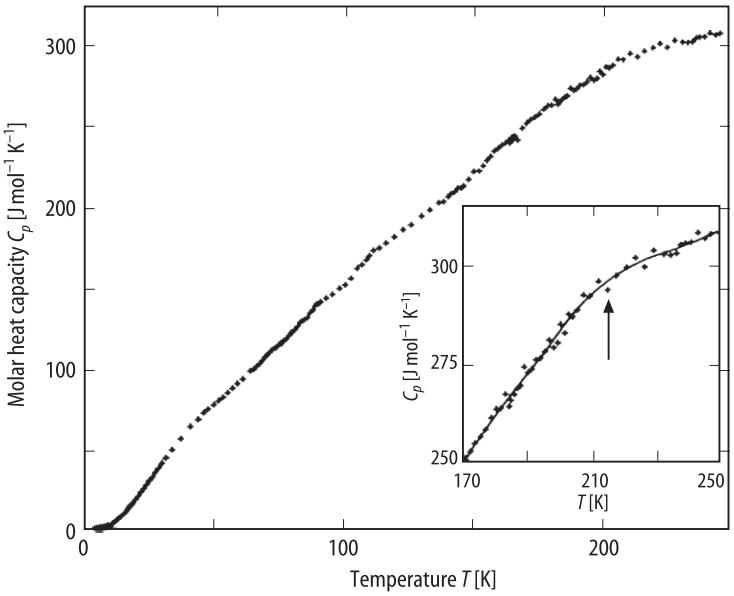

Fig. 65A-3-016. $(CH_3)_3NCH_2COO \cdot H_3PO_3$ (BPI). C_p vs. T [93Feh]. C_p: molar heat capacity at constant pressure. The arrow in the insert indicates Θ_{III-II} determined in dielectric measurements.

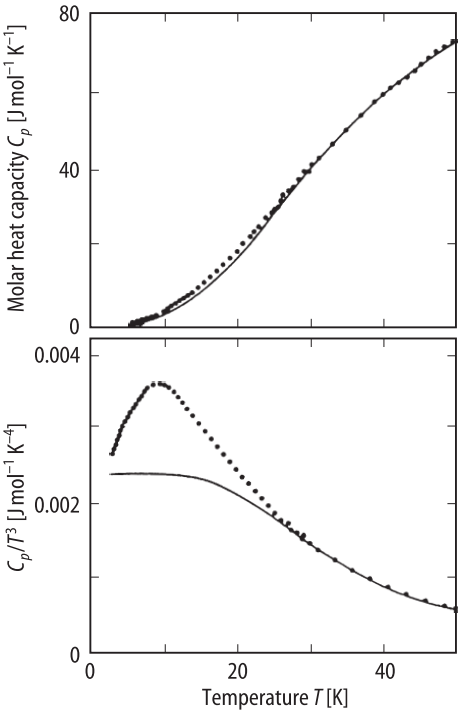

Fig. 65A-3-017. $(CH_3)_3NCH_2COO \cdot H_3PO_3$ (BPI). C_p vs. T, C_p/T^3 vs. T in the low temperature region [93Feh]. C_p: molar heat capacity at constant pressure. The solid lines are calculated using the Debye model for the specific heat with Debye temperature Θ_D = 154 K.

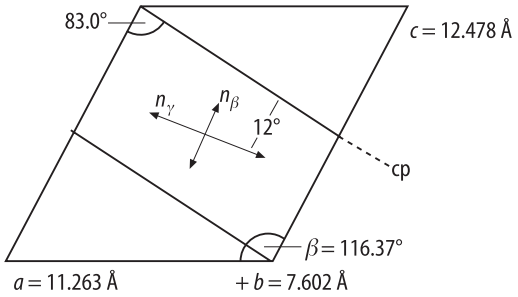

Fig. 65A-3-018. $(CH_3)_3NCH_2COO \cdot H_3PO_3$ (BPI). Orientation of the principal axes of indicatrix and the cleavage plane cp (|| to $(10\bar{2})$) [88Alb1]. Fat lines: natural faces.

References

88Alb1 Albers, J., Klöpperpieper, A., Rother, H.J., Haussühl, S.: Ferroelectrics **81** (1988) 27.

88Alb2 Albers, J.: Ferroelectrics **78** (1988) 3.

89Dor Dörffel, M., Narz, Th., Haussühl, S.: Z. Kristallogr. **186** (1989) 71.

92Lau Launer, S., LeMaire, M., Schaack, G., Haussühl, S.: Ferroelectrics **135** (1992) 257.

92Vol Völkel, G., Pöppl, A., Metz, H., Klöpperpieper, A.: Ferroelectrics **125** (1992) 11.

93Bau Bauch, H., Böttcher, R., Völkel, G.: Phys. Status Solidi (b) **179** (1993) K41.

93Feh Fehst, I., Paasch, M., Hutton, S.L., Braune, M., Böhmer, R., Loidl, A., Dörffel, M., Narz, Th., Haussühl, S., McIntyre, G.J.: Ferroelectrics **138** (1993) 1.

93Sob Sobiestianskas, R., Grigas, J., Czapla, Z., Dacko, S.: Phys. Status Solidi (a) **136** (1993) 223.

95Cac Cach, R., Backo, S., Czapla, Z.: Phys. Status Solidi (a) **148** (1995) 585.

95Ebe Ebert, H., Lanceros-Méndez, S., Schaack, G., Klöpperpieper, A.: J. Phys. Condens. Matter **7** (1995) 9305.

96Ban Banys, J., Sobiestianskas, R., Völkel, G., Klimm, C., Klöpperpieper, A.: Phys. Status Solidi (a) **155** (1996) 541.

96Fre Freude, P., Michel, D.: Phys. Status Solidi (b) **195** (1996) 298.

97San Santos, M.L., Almeida, A., Chaves, M.R., Klöpperpieper, A., Albers, J., Gomes-Moreira, J.A., Gervais, F.: J. Phys. Condens. Matter **9** (1997) 8119.

98Fre Freude, P., Totz, J., Michel, D., Arndt, M.: J. Phys. Condens. Matter **10** (1998) 429.